MODEL STUDY OF TUYERE EROSION

IN REFINING

BY

TOMLINSON KOMANI HARA B.Min.Sc.

A dissertation submitted to the University of Zambia in partial fulfilment of the requirements of the degree of Master of Mineral Sciences in Metallurgy and Mineral Processing.

THE UNIVERSITY OF ZAMBIA

LUSAKA

1986

DECLARATION

I declare that this dissertation represents my own work and that it has not previously been submitted for a degree at this or another University.

Where other people's work has been incorporated, acknowledgement has been made.

Signature of Author: ....

Date: 11th NOVEMBER 1986

This dissertation of Tomlinson Komani Hara is approved as fulfilling part of the requirements for the award of the degree of Master of Mineral Sciences in Metallurgy and Mineral Processing by the University of Zambia.

Signatures of Examiners:	Date:
1 ..R. Harris...................... DR. R. HARRIS	Dec. 18, 1986
2 .... DR. J.B. MWALULA	22nd June, 1987
3 ..E.H. Jere.................. DR. E.H. JERE	22/6/87

DEDICATED

TO

MY LATE DAD, THE BEST AND PERFECT
DAD ONE COULD EVER HAVE.

I MISS YOU.

SYNOPSIS

The erosion of Tuyeres in Refining has been studied in a Physical Model to establish the dependence upon injection conditions such as gas momentum and orifice profile. The erosion phenomena in terms of Mass transfer-mechanisms has also been studied.

A coefficient of Mass transfer k_{α}, has been determined to accommodate the fluctuating nature of the flow. This has been found to be dependent on gas injection rate at a particular nozzle diameter.

The dependence of the erosion mechanism on the original orifice diameter has been determined. A relationship of the final diameter with the Modified Froude Number and the original orifice dimensions has been defined. The rate at which the diameter increases with time has also been determined.

The final bubble contact radius has been found to be influenced by the high gas momentum and kinetic energy which promote erosion, as such lateral erosion which is the erosion due to the washing or spreading effect of the bubble growth also depends on these.

Axial erosion has been found to be affected mostly by inertial forces. It is also dependent on the amount of liquid entrained in the Tuyere. Two-phase flow experiments show that liquid entrained in a Tuyere is to a great extent dependent on the gas flowrates in use. As the process approaches jetting conditions, the percent volume liquid entrained is greatly reduced. Bubble detachment has also been found to affect axial erosion.

ACKNOWLEDGEMENTS

I wish to thank Dr. A.E. Wraith of the Department of Metallurgy and Engineering Materials at the University of Newcastle-Upon-Tyne (UK) under whom this project was carried out, for all the help, encouraging words, and for his general contribution and concern in enabling me understand Process Modelling and Engineering.

I would like to thank Dr. J.B. Mwalula my supervisor at University of Zambia for all the constructive comments. I also thank Dr. J.D. Gilchrist and Dr. E.H. Jere for their comments on the text. Thanks are also due to all members of staff in the Department of Metallurgy and Engineering Materials at University of Newcastle-Upon-Tyne and the Research group, who helped in one way or the other. I also thank Mrs. M. Sanga for typing the work.

I am greatly indebted to the British Council and the University of Zambia for the sponsorship of my studies at Newcastle University.

Very special thanks go to Mum, Yobe, Lilian and Sydney for their encouragement, Love and Care.

God Bless You All.

CONTENTS PAGE

CONTENTS PAGE

CHAPTER TWO

CONTENTS

PAGE

CHAPTER THREE

CHAPTER FOUR

CONTENTS

LIST OF FIGURES AND TABLES

FIGURES

TABLES

NOTATION

CHAPTER 1 and 3

SYMBOL	DESCRIPTION	DIMENSIONS
A_c	Cross-section area of the gas core	L^2
a	Hemispherical bubble radius	L
d	Diameter of pipe	L
d_b	bubble diameter in contact with surface	L
d_o	Orifice diameter	L
F	Pressure function	$L^2 T^{-2}$
F_B	Buoyant force	MLT^{-2}
F_M	Momentum force	MLT^{-2}
F_R	Reaction at the base of expanding hemispherical bubble	MLT^{-2}
g	acceleration due to gravity	LT^{-2}
k_1	Constant of proportionality	-
N^*_{Fr}	Modified Froude Number	-
N_I	Injection Number	-
P	Pressure at radial point in liquid	$ML^{-1} T^{-2}$
P_H	Gravitation pressure	$ML^{-1}T^{-2}$
P_I	Inertial pressure	$ML^{-1}T^{-2}$
P_o	local hydrostatic pressure	$ML^{-1}T^{-2}$

SYMBOL	DESCRIPTION	DIMENSIONS
P_s	Surface pressure	$ML^{-1}T^{-2}$
P_θ	Pressure at (a, $\underline{\theta}$) on a hemispherical bubble	$ML^{-1}T^{-2}$
Q	volumetric flowrate	L^3T^{-1}
q	absolute liquid velocity	LT^{-1}
R	radial distance from bubble centre	L
r_o	Orifice radius	L
r_c	bubble contact radius	L
S	distance of displacement of bubble centre above orifice	L
V	volume	L^3
t	growth time	T
v_o	orifice gas velocity	LT^{-1}
v_g	average velocity of gas core	
ρ	density	ML^{-3}
ϕ	velocity potential	L^2T^{-1}
γ	liquid interfacial tension	MT^{-2}
ν	kinematic viscosity	L^2T^{-1}
μ	dynamic viscosity	$ML^{-1}T^{-1}$
δ_ℓ	liquid film thickness (normally the mean value)	L

Subscripts

G, g = gas

L, ℓ = liquid

h = refering to hemispherical bubble at its maximum size

B, b = bubble

CHAPTER 2

SYMBOL	DESCRIPTION	DIMENSIONS
A	Surface area from which particles are diffusing	L^2
C	molar density of fluid	moles L^{-3}
C_{Ai}	concentration at position i	moles L^{-3}
C_{Ao}	initial concentration	moles L^{-3}
C_b	bulk concentration	moles L^{-3}
$\bar{C}$	time average concentration	moles L^{-3}
(C_B) lm	logarithmic mean concentration of non-diffusing species B	moles L^{-3}
C_{sat}	saturated concentration	moles L^{-3}
C_{eq}	Equilibrium concentration of bath	moles L^{-3}
$\Delta C = C_{sat} - C_{eq}$	Concentration driving force	moles L^{-3}
D	Diffusivity	L^2T^{-1}
D_{AB}	Diffusion coefficient, which is a measure of the diffuse mobility of species A in B	$L^2\ T^{-1}$
D_E	eddy diffusivity	$L^2\ T^{-1}$
j	mass flux per unit area	$ML^{-2}T^{-1}$
K, k_m	mass transfer coefficient	LT^{-1}
k_d	diffusion coefficient	LT^{-1}

SYMBOL	DESCRIPTION	DIMENSIONS
k_α	arbitrary 'erosion' mass transfer coefficient, $k_\alpha = k_m A$	$L^3 T^{-1}$
N_A	molar flux of diffusing species A	moles $L^{-2}T^{-1}$
n	moles being transferred from area A in time t	moles
$\dot{n}$	rate of dissolution	moles T^{-1}
S_c	Schmidt Number	-
U_x, U_y	velocity in x and y coordinates	LT^{-1}
V_{str}	maximum stream velocity	LT^{-1}
$\bar{V}_x$	instantaneous flow velocity of stream	LT^{-1}
X_A	mole fraction of A	-
X_{Ao}, X_{Ab}	mole fraction of A at surface and at the outer edge of the fluid	-
$(X_B)_{lm}$	logarithmic mean of the initial and final mole fraction of companent B (non-diffusing)	
ρ	density	ML^{-3}
ν	kinematic viscosity	L^2T^{-1}
μ	dynamic viscosity	$ML^{-1} T^{-1}$
δ	thickness of 'stagnant' layer	L
δ_d	diffusional boundary layer thickness	L

Subscripts

b	bulk
i	at the interface
r	radial
Sat	saturated
Str	stream
Z	axial

Data for computation

$g = 9.81\, m^2/s$

$\pi = 3.1415927$

$\rho_{He} = 0.1664\ kg/m^3$ at $20^\circ C$ and 1 atmosphere

$\rho_{HCl\,(aq)} = 1020\ kg/m^3$ at $20^\circ C$ and 1 atmosphere.

$\rho_{Air} = 1.204\ kg/m^3$ at $20^\circ C$ and 1 atmosphere

$\rho_{H_2O} = 1000\ kg/m^3$ at $20^\circ C$ and 1 atmosphere

$\rho_{Cu} = 7990\ kg/m^3$ at $1083 \pm 0.2^\circ C$

$\rho_{Fe} = 7030\ kg/m^3$ at $1535^\circ C$.

$D_{AB} = 1.0 \times 10^{-5}\ m^3/s$

INTRODUCTION

In nearly all metal extraction processes, when an ore has been smelted, there is need for the product metal to be refined further to meet certain composition requirements by the customer. In both steel-making and Copper converter practice, impurities like sulphur and phosphorus are oxidised in order to get a purer metal.

The refining practice in use by most smelters is to refine the metal while it is in its molten state by using gases, for example Air and Oxygen. The gas is injected into the melt either by lancing or submerged bottom blowing. The gas creates an interfacial area for the refining reaction to proceed. The injection of the gas as applied to conventional copper converters is by bottom blowing of the refining gas into the Copper matte through Tuyeres which are basically metal pipes. The rate of refining depends on the rate of gas injection. The tendency in most plants is to use high flowrates, which lead to erosion of the Tuyeres, for example in copper refining $13m^3/min$ is used whereas in iron and steel making 55 m^3/min is used. The wear of the Tuyeres takes place both on the top surface wall and in the bore (inner part) and it creates operational difficulties and increases costs as relining usually depends on Tuyere wear.

The aim of the present work was to find out how erosion depends on injection conditions such as gas momentum and orifice profile, and to determine any erosion regimes in terms of Mass-Transfer mechanisms.

The experimental model used in this work was that of a bottom blown Tuyere acting vertically upwards as in bottom blown metal converters. Model soluble Tuyere panels were tested in a transparent isothermal half-slice model to elucidate the erosion effects. It was found convenient to use the upward acting Tuyere as it is fairly well understood and the results obtained could be modified to apply to the Tuyeres of other orientations. Constant gas flow conditions are used, and the same can be assumed to apply in actual situations.

The literature review begins with a survey of bubble formation at the orifice, as the formation of bubbles influences the erosion profiles of the Tuyeres. Literature on Mass Transfer from the eroding solid phase to the bulk of the melt has been reviewed. The gas-liquid interaction, effect of recirculating currents have been reviewed and studied.

In the theory of bubble formation at the Tuyere Orifice in submerged gas injection, factors influencing bubble behaviour have been explained to some extent. Work has been carried out by many workers to determine the effect of submerged jets on flat surfaces in terms of hydrodynamics of flow in general and to some extent the Mass transfer mechanism from and to the surface of the solid plates.

Most of the work has been carried out using water-air systems and correlations could in some way be made to physical situations encountered in most Metallurgical and Chemical Engineering processes. If we consider that molten metals like copper and molten iron have densities of approximately eight times that of water, the gas-liquid ratio in converters will be much lower. It was found necessary to use a system of nearly the same density ratio as that in the actual Metallurgical operations.

In the present work, the Helium - Hydrochloric Acid - $(CaSO_4)_2$ H_2O system was used which gave nearly the same gas to liquid density ratio as that of the gas to metal system used in modern copper and iron industries. For example:

$$\frac{\rho_{He}}{\rho_{HCl}} = 1.63 \times 10^{-4} \; ; \; \frac{\rho_{O2}}{\rho_{Fe(l)}} = 1.9 \times 10^{-4} ; \; \frac{\rho_{Air}}{\rho_{Cu(l)}} = 1.51 \times 10^{-4}$$

as such the system could be said to be representative of the actual operating conditions in commercial practice.

The acceptable ranges of Injection Number 0.05 to 0.06 and Modified Froude Number 10 to 200 as applied to industrial practice were used.

LITERATURE REVIEW

CHAPTER ONE

INTRODUCTION

The formation of bubbles and flow patterns of gas injected through submerged horizontal nozzles depends on a number of principal factors such as; flowrate, gas orifice diameter, orifice dimensions and others like liquid viscosity, liquid density, surface tension and the Injection Number. These will be considered in the following sections:

1.0 MECHANISM OF BUBBLING AND JETTING

(Bubble Formation Theory)

When a gas is injected through a submerged flat nozzle, bubbles form at the orifice and move upwards due to buoyancy[2]. The formation of the bubbles and the wall interaction is dependent mainly upon the injection number N_I, injection rate, nozzle geometry and the fluid properties.

Two models which explain the growth of bubbles from an orifice are discussed in the following sections.

1.1 The Davidson and Schüller Model[6]- Bubble Growth

Considering constant flowrates, these workers state that, for bubbles to form, the pressure p_1 in the vessel below the orifice plate must exceed a minimum value equal to the sum of the static head of liquid, h, above the plate plus a surface term $2\sigma/r_o$. The theory and experiments confirm that if the vessel below the orifice plate is large, then as soon as p_1 is greater than $\rho gh + 2\sigma/r_o$, bubbles of a finite size will form continuously, so that the gas flowrate suddenly increases from zero to a finite amount.

i.e. $p_1 > p_s + p_H + p_o$ (1)

(for growth to occur)

Assuming that the bubble is spherical at all times during formation and its upward motion is determined by a balance between buoyancy force and upward mass acceleration of the fluid surrounding the bubble,

the equation of upward motion is

$$Vg = \frac{d}{dt}\left(\frac{11}{16} V \frac{ds}{dt}\right) \qquad (2)$$

With a constant gas flowrate Q and an initial bubble volume of zero and V = Qt, by substitution in (2) the equation can be integrated.

When

$$t = 0, \quad \frac{ds}{dt} = 0$$

and assuming that the bubble growth is terminated when its radius r equals s the distance travelled, we obtain the final bubble volume as

$$V_1 = 1.378\ Q^{6/5}.\ g^{-3/5} \qquad (3)$$

V_1 = Bubble volume just before detachment

As each bubble breaks away from the orifice, it leaves behind a volume of gas V_o which becomes a site for the next bubble. In the derivation of equation (2) it is assumed that V_o is much less than V_1, but with larger orifices V_o is not negligible and it is necessary to take bubble volume at time t as

$$V = \frac{4}{3}\pi r^3 = Qt + V_o \qquad (4)$$

V = Bubble volume at time t

$V_o = 4\pi ro^3/3$

When integrating equation (2) , this gives, with the initial conditions:

$$t = 0; \quad s = \frac{ds}{dt} = 0$$

$$S = \frac{16}{11}g\left[\frac{t^2}{4} + \frac{V_o t}{2Q} - \frac{V_o^2}{2Q}\ln\left(\frac{Qt + V_o}{V_o}\right)\right] \qquad (5a)$$

In this case the bubble is assumed to detach when $S = r + r_o$ and the lifetime of the bubble is obtained by plotting equation (5a) and plotting $r + r_o$ as a function of time from equation (4) on the same axes.

Equations (3) and (4) are classified according to flowrates

1) For small flowrates

$$V = 1.378\, Q^{6/5}\, g^{-3/5} \qquad (3)$$

2) For large flowrates (4) and (5a) are used

$$V = \frac{4\pi r^3}{3} = Qt + V_o = Qt + \frac{4\pi r_o^3}{3} \qquad (4)$$

The point source bubble formation considered by Davidson et al in developing the above equations is shown in Fig. 1.

1.2 Bubble Growth - Wraith's Model [1]

The model describes the process of the gas emerging into bubbles as shown in Fig. 2.

Bubbles continue to grow and expand in two stages. Wraith et al[1] developed equations for determining the maximum attainable radius and volume for an expanding bubble before and at detachment. The following assumptions were employed in developing the equations:-

1) Surface tension was neglected

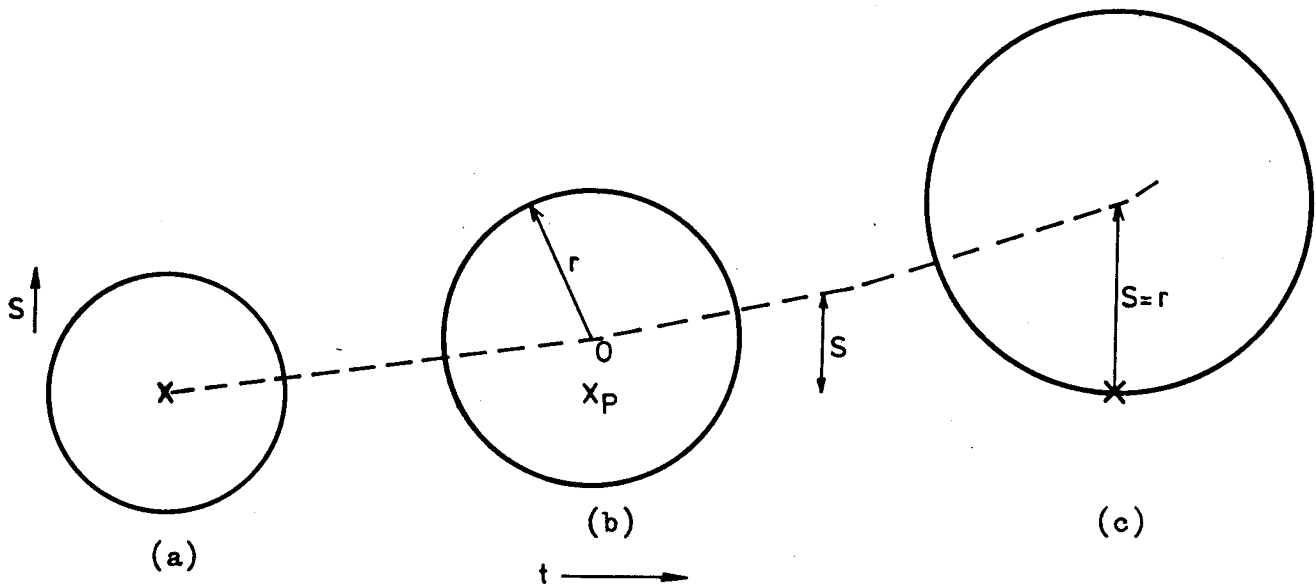

(a) Underside of bubble moving down

(b) Bottom point of bubble at rest in lowest point

(c) Bottom point of bubble reaches gas source (ideal detachment).

Fig. 1 SCHEMATIC REPRESENTATION OF POINT SOURCE BUBBLE FORMATION

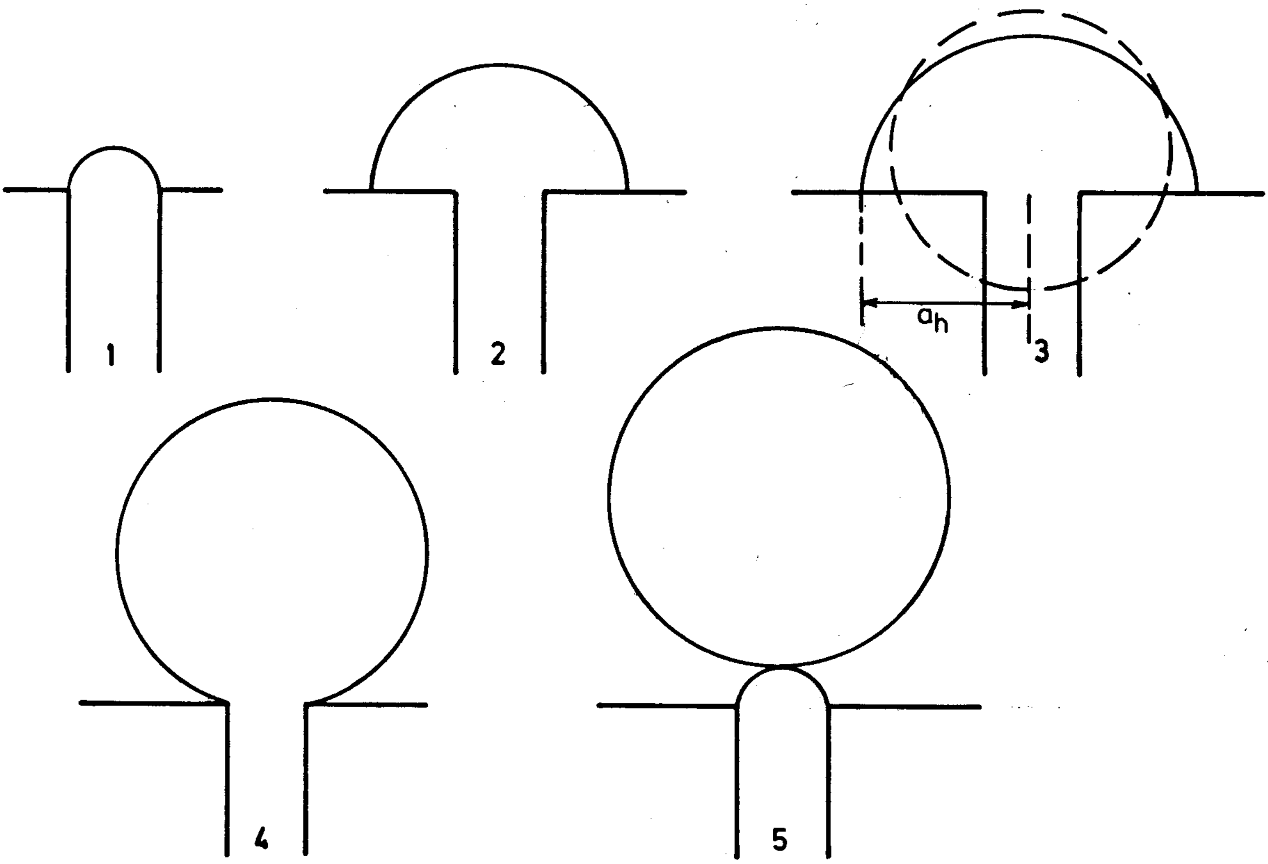

3) Shows the transition from the hemispherical, stage 1, to the spherical stage 2

5) Shows the detachment position.

Fig. 2 A Schematic representation of bubble shape during the two stage growth process

2) The gas injection rate was constant and the gas incompressible
3) Liquid was inviscid and large extent
4) The gas bubble surface was spherical.

Another assumption considered was that the gas at the orifice is taken from a point source at the centre of bubble as suggested by Davidson et al[2].

The basic equation used was the pressure equation which deals with pressure in liquid associated with expansion

$$\frac{P}{\rho_l} + \frac{q^2}{2} - \frac{\partial \phi}{\partial t} = F(t) \qquad (5b)$$

Considering a stationary expanding sphere of radius r,

$$\phi = \frac{r^2}{R} \frac{dr}{dt} \quad (6), \qquad q = \frac{r^2}{R^2} \frac{dr}{dt}, \quad R >> r \qquad (7)$$

When the source has constant flowrate Q (m^3/s)

Velocity potential $\phi = \frac{Q}{4\pi R}$ m^2/s (8)

and

$$\frac{\partial \phi}{\partial t} = \frac{r^2}{R} \left(\frac{d^2 r}{dt^2}\right) + \frac{2r}{R}\left(\frac{dr}{dt}\right)^2 = 0 \qquad (9)$$

On substituting in (5b) and further assuming that the pressure at infinity is negligible, F(t) = 0

$$\frac{P}{\rho_l} + \frac{1}{2}\frac{r^4}{R^4}\left(\frac{dr}{dt}\right)^2 = 0 \qquad (10)$$

g is neglected when considering that $d^2r/dt^2 \gg g$ which is the case when r is small and Q is large, as given by Schüller and Davidson.[6]

Since the constant flow gas source is located close to the rigid surface of a horizontal rigid plate, the spherical symmetry exhibited by a rapidly expanding envelope will be confined by the plate to one of the hemispherical radial growth. For such an envelope at constant Q, the radial velocity is

$$\frac{da}{dt} = \frac{Q}{2\pi a^2} \qquad (11)$$

with a as the hemispherical radius.

The pressure P_e due to expansion alone at the hemispherical surface, R = a, is given by substituting (11) into (10).

$$\left(\frac{da}{dt}\right)^2 = \frac{Q^2}{4\pi^2 a^4} \Rightarrow \frac{P_e}{\rho_l} + \frac{1}{2}\frac{Q^2}{4\pi^2 a^4} = 0$$

$$\frac{P_e}{\rho_l} + \frac{1}{8}\cdot\frac{Q^2}{\pi^2 a^4} = 0 \qquad (12)$$

The equation of equilibrium for the expanding hemisphere is established by setting equal to zero the sum of the reactive forces F_R due to the plate and the force on the expanding surface due to the components of the surface pressure P_θ in the liquid, See Fig. 3.

From Figure 3

$$F_R - 2\pi a^2 \times \int_0^{\pi/2} P_\theta \cos\theta \sin\theta d\theta = 0 \qquad (13)$$

P_θ has two components

1) due to expansion P_e (assumed independent of g)

2) Hydrostatic pressure at (a, θ)

$P_o - \rho_\ell g\, a \cos\theta.$

Where

P_o = pressure at the plate surface when there is no expansion

Therefore we have

$$P_\theta = \frac{\rho_\ell Q^2}{8\pi^2 a^4} + P_o - \rho_\ell g a \cos\theta \qquad (14)$$

Substituting into (13) and integrating we obtain

$$F_R - 2\pi a^2 \left(\frac{\rho_\ell Q^2}{16\pi^2 a^4} + \frac{1}{2} P_o - \frac{1}{3} \rho_\ell g a \right) = 0 \qquad (15)$$

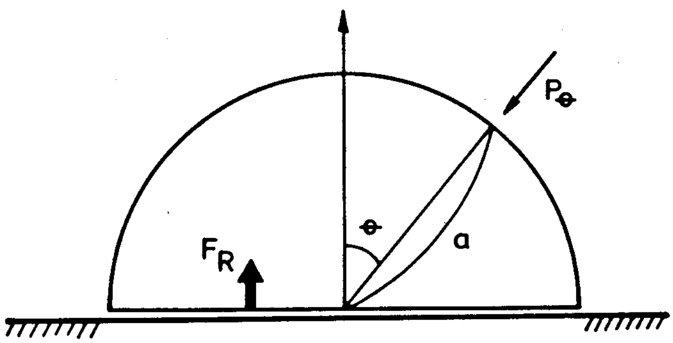

Fig. 3 Configuration of an expanding hemispherical bubble

If $F_R \geqslant \pi a^2 P_o$ the bubble remains in equilibrium and in contact with the plate. When F_R is less than hydrostatic force on the base surface, the bubble goes up. As such the limiting conditions for equilibria are

$$\frac{\rho_l Q^2}{8 \pi a^2} = \frac{2}{3} \pi a^3 \rho_l g \qquad (16)$$

$$a_h^5 = \frac{3Q^2}{16 \pi^2 g} \qquad (17)$$

a_h = hemispherical radius

giving the maximum attainable radius by a stable hemispherical bubble as

$$a_{max} = a_h = 0.453 Q^{2/5} . \ g^{-1/5} \qquad (18)$$

with the bubble volume as

$$V_h = 0.194 \ Q^{6/5} . \ g^{-3/5} \qquad (19)$$

These equations are for the first stage of the bubble formation. Bubble growth beyond V_h constitutes the second stage in achievement of detachment volume.

In developing the equation for the second stage of the bubble formation it was assumed that at constant flowrate,

$$V = Q\ (t + t_h) \tag{20}$$

where,

$$t_h = \frac{V_h}{Q} \tag{21}$$

and these were used in the force equation by Schüller [6].

$$\frac{16}{11}\ g(t + t_h) = \frac{d}{dt}\left[(t + t_h)\ \frac{ds}{dt}\right] \tag{22}$$

and considering that the centre of mass of a hemisphere is located at a polar height of 3/8a. above the base, the volume of detachment was found by integrating equation (22), where

$$s = 3/8a \qquad \text{at } t = 0$$

and letting s equal to the bubble radius at detachment. Therefore

$$s = \left(\frac{3}{4}\ \frac{Q}{\pi}\ (t + t_h)\right)^{\frac{1}{3}} \tag{23}$$

The general solution for the volume of the bubble was found to be of the form,

$$V = kQ^{6/5}.\ g^{-3/5} \tag{24}$$

growth time would be

$$t = \frac{V}{Q} = kQ^{1/5}.\ g^{-3/5} \tag{25}$$

On substituting

$$t + t_h = kQ^{1/5}.\ \ g^{-3/5} \tag{26}$$

and from (19)

$$t_h = 0.194Q^{1/5}.\ \ g^{-3/5}$$

k was obtained as

$$k = 1.090 \text{ and}$$

$$V = 1.090Q^{6/5} . \; g^{-3/5} \qquad (27)$$

This equation had some similarity with those developed by Davidson and Schüller and by Walters and Davidson[13].

In case of sidewall injection,

$$V = 1.306Q^{6/5} \; g^{-3/5} \qquad (28)$$

For the second stage to occur, a_h must be larger than the orifice r_o. There exists a critical flowrate for $a_h = r_o$

$$Q_{crit} = \frac{r_o^{5/2} . \; g^{1/2}}{(0.453)^{5/2}} = 7.25 \, r_o^{5/2} \; g^{1/2} \qquad (29)$$

which is the lowest flowrate at which the two stage model is applicable, as such flowrates should always be greater than Q_{crit} for bubbles to form.

The minimum flowrate for incipient coalescence at the orifice between the detaching and newly forming bubble was found to be;

$$Q = 7.44 \; r_o^{5/2} . \; g^{1/2} \qquad (30)$$

1.3 Bubble Pressure

As the bubbles expand radially, they possess an internal pressure P_b due to liquid inertia, surface tension and gravity effects.

$$P_b = P_H + P_I + P_s + P_o \qquad (31)$$

This is given as

$$P_b = -\rho_l g s + \frac{\rho_l Q^2}{32\,\pi^2 a^4} + \frac{2\gamma}{a} + P_o \qquad (32)$$

In the hemispherical stage P_b is given as

$$P_b = -\frac{3}{8}\rho_l g a + \frac{\rho_l Q^2}{8\,\pi^2 a^4} + \frac{2\gamma}{a} + P_o \qquad (33)$$

$\frac{2\gamma}{a}$ is negligible at high flowrates [2].

P_b reaches a maximum when $a = r_o$. As $\underline{a}$ increases it reaches a value when the bubble is severed from the gas supply.

Chalkley and Wraith [3] studied the bubbling process and three bubble regimes were established prior to severence of the bubbles; These were Triple formation, Binary coalescence and Stem coalescence, and exist in order of increasing injection rate.

1) In triple formation, successive bubbles are joined together and coalesce at a distance above the orifice before cut-off. See Plate 2.

2) Binary coalescence with stem formation, in which gas supply to a fully developed bubble didn't appear to be interrupted.

3) Stem coalescence, during this process the point of contact between successive envelopes of the binary coalescence regime reached down to the orifice and the dispersion gas stream became an irregular sequence of coalesced elongated envelopes.

The bubble formation sequence in the two stage process is shown in Fig. 2. Bubble coalescence regimes can be seen from Plate 2.

It was found that the cut-off volume, is given by

$$V = 1.54\, Q^{6/5} \cdot g^{-3/5} \qquad (34)$$

The momentary cut-off occurs at high flowrates[4] when the stem connecting the orifice to the bubble is severed due to flow and pressure fields in the wake of the rising bubble [5].

2.0 PARAMETERS AFFECTING BUBBLE GROWTH [2]

(effect of Physical variables)

Introduction

In this section effects of several relevant parameters affecting bubble growth will be discussed separately.

2.1 Constant gas flowrates and supply pressure of gas

Davidson and Schüller[2] found that the volume of a bubble at an orifice submerged in a viscous liquid could be calculated by assuming that the orifice acted as a point source of gas supply and that the motion and position of the bubble is governed by viscosity, inertia and buoyancy. See Fig. 1.

They distinguished two cases

a) constant gas flowrate

b) constant supply pressure of gas.

In both cases the forces due to inertia were negligible if the overall gas flowrate was small.

For a constant gas flowrate, the volume of the bubble that detaches is a function of the gas flowrate and the kinematic viscosity of the liquid. In this case, the effect of dimensions of the orifice is negligible.

For constant gas pressure, the orifice dimensions are important and the volume of the bubble is a function of a constant dependent on size and shape of orifice, density of the gas, kinematic viscosity and pressure of gas supply. In this case the average gas flowrate is a dependent variable which is affected by all factors which influence the bubble volume. The bubble formed in this case receives a great portion of its gas during the detachment period[6].

2.2 Effect of Viscosity

From Stoke's law

$$V = \frac{2r^2g}{9\nu} = \frac{2r^2g\rho}{9\mu} \qquad (35)$$

The velocity of a bubble rising is inversely proportional to the viscosity and since the volume of a bubble forming above an orifice depends on the time it is in contact with the orifice, the viscosity could have an effect on the bubble size. But, the effect is very small in metal melts and can be ignored as far as it influences bubble growth.

2.3 Effect of Gas Flowrate

At any particular viscosity, the frequency of bubble formation is nearly constant, and changes in gas flowrate merely change the volume of individual bubbles.

2.4 Effect of Orifice dimensions

At constant gas flowrates and gas supply pressure the flow through an orifice is proportional to its cross-sectional area.

2.5 Effect of Liquid Density

With constant gas flowrates an increase in the density of the liquid has the effect of increasing the velocity with which the bubble rises and a smaller bubble results. With constant pressure, the density of the liquid also has an effect on the gas flowrate into the bubble. As the bubble rises, the hydrostatic head, which depends on the density of liquid decreases. The pressure in the bubble becomes less and the gas flowrate into it increases.

2.6 Effect of Surface Tension

The effect of surface tension, depends on the magnitude of flowrate Q, and the original orifice diameter d_o. When the gas flowrate is constant, the surface tension has no effect other than due to the small forces arising from contact around the edge of the orifice. The surface tension effects are usually small in big bubbles which exist in most metallurgical systems.

2.7 Effect of Gas Density

Gas density is only important with constant pressure supplies when it affects the discharge of gas through the orifice.

The effect of liquid inertia at start of bubble growth as studied by Robertson and Nilmani[7] at constant flowrate conditions is such that the flow into the bubble will intially be slow and will increase later to a constant maximum value.

3.0 THE INJECTION NUMBER, N_I AND MODIFIED FROUDE NUMBER, N^*_{Fr}

The injection number, is a ratio of the forces acting on the gas bubble in representation of momentum effects on the bubble. The forces are, the momentum force and the Buoyancy force. It is given as;[12]

$$N_I = \left[\frac{Q^2}{r_o^5 g}\right]^{2/5} \times \frac{\rho_g}{\rho_\ell} = \left[\frac{\pi^2 V_o^2}{r_o g}\right]^{2/5} \times \frac{\rho_g}{\rho_\ell} \quad ($$

Representation of Momentum[9]

See Fig. 4

$$\frac{F_M}{F_B} = \frac{\text{Momentum force}}{\text{Buoyancy force}} \qquad (37)$$

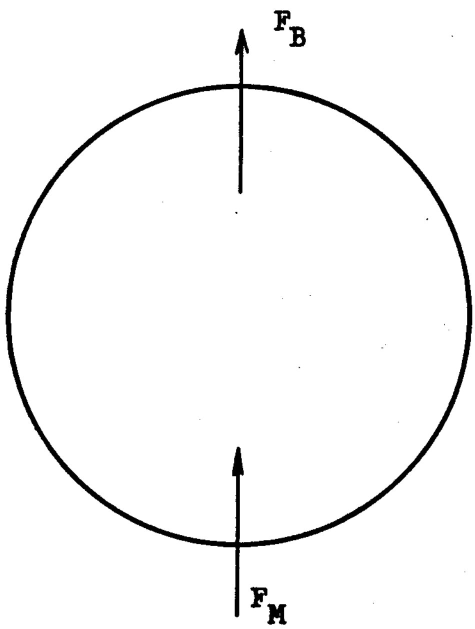

$$\frac{F_M}{F_B} = \frac{\text{Momentum force}}{\text{Buoyant force}}$$

Fig. 4 Representation of momentum

In terms of flowrate Q, (L^3T^{-1})

$$F_M = \frac{\rho_g Q^2}{\pi r_o^2} \tag{38}$$

$$F_B = V_B \rho_\ell g = k_1 \rho_\ell Q^{6/5} \cdot g^{2/5} \tag{39}$$

Therefore equation (37) becomes

$$\frac{F_M}{F_B} = \frac{1}{\pi k_1} \times \left(\frac{\rho_g}{\rho_\ell}\right) \times \frac{Q^{4/5}}{r_o^2 \quad g^{2/5}}$$

$$\frac{F_M}{F_B} \cong \frac{\rho_g}{\rho_\ell} \left(\frac{Q^2}{r_o^5 g}\right)^{2/5} = N_I$$

In this equation, the ratio ρ_g/ρ_ℓ is very crucial especially when using other fluids to represent what happens in the actual plant operations. The Injection Number is the basis for comparing the Air/Water or Helium/Hydrochloric acid systems with the highly energetic injection of refining gases in melts.

Bubbles in submerged gas injection, form only in the range of Injection Numbers 0 to 0.1. Beyond 0.1, jetting behaviour is apparent.

Variation of Injection Number with volume of bubble is given in Fig. 5.

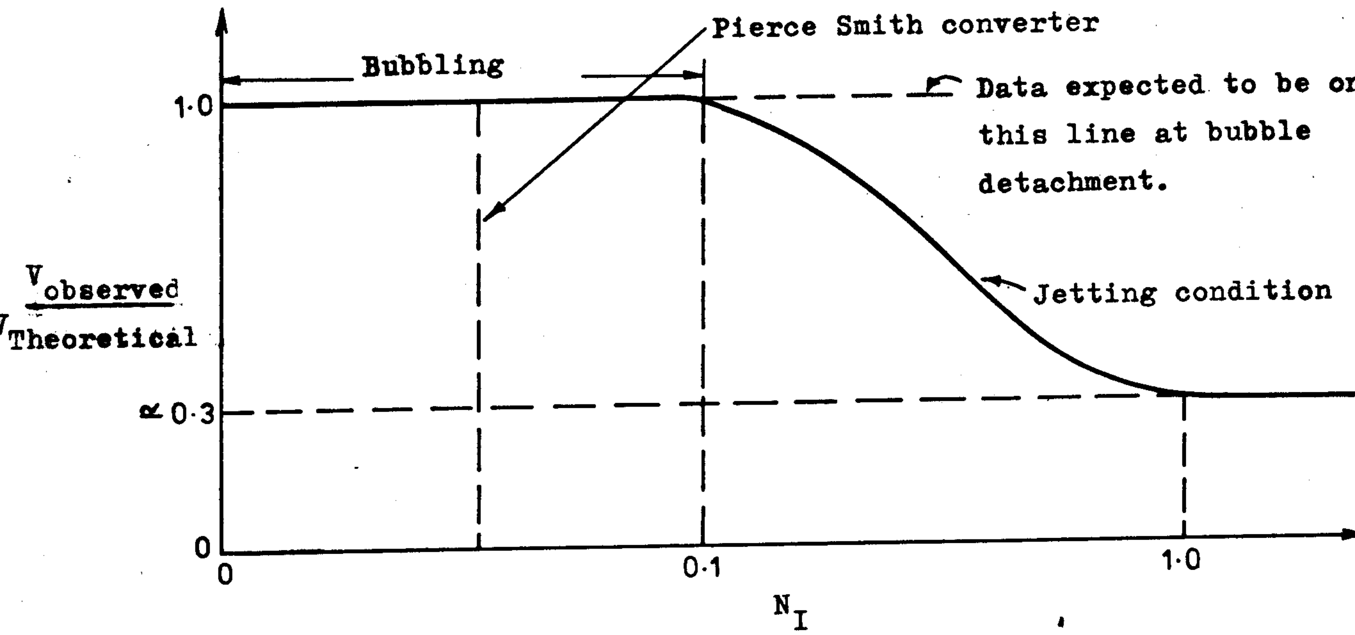

Fig. 5 Variation of bubble volume with injection

For copper converters $N_I \cong 0.06$ (almost ideal behaviour). The frequency of bubble formation is 7 to 80 Hertz. In Fig. 5; $N_I = 0.1$ is the point of diversion.

Jetting condition:- In this region the number of bubbles becomes less and eventually no bubbles are obtained.

In the above mentioned case, increase in the flow-rate was found to lead to a succession of continuous coalescence regimes of bubbles.

There is also the modified Froude Number,[14] N^*_{Fr}. This is the ratio of the inertial forces to the gravitational forces, and it describes fluid flow behaviour in gas-liquid systems where the liquid surface is wavy and curved. It gives an idea of the type of flow existing in a system. It is defined as

$$N^*_{Fr} = \frac{\rho_g V_o^2}{\rho_l g . d_o} = \frac{\text{Inertial force}}{\text{Gravitational force}}$$

CHAPTER 2

MASS TRANSFER

INTRODUCTION

The review looks at erosion in general from a solid surface and the material transported into the bulk of the liquid. In Tuyere erosion mass transfer occurs when particles eroded from the solid tuyere surface go into the melt.

In submerged tuyere gas injection, the transfer of mass is by forced convection from the solid flat surface into the bulk of the bath.

1.0 CONVECTIVE MASS TRANSFER

In convective mass transfer, the transport of a given species by diffusion is modified by the bulk motion of the fluid in which the diffusive process occurs. When the flow field is imposed by external forces, mass transfer is said to occur by means of forced convection. An example of this is that of gas injection through a tuyere from a compressed air source.

2.0 BOUNDARY LAYER THEORY

In the flow of a fluid past a phase boundary, across which mass transfer occurs, there will be a velocity gradient within the fluid which results in a transfer of momentum through the fluid [17].

Since fluids adhere strongly to solid surfaces, the fluid immediately adjacent to the solid surface is always at rest. See Fig. 6 and 7. Between the solid surface and some point far out into the fluid stream, the flow velocity $\bar{V}_x$ of the fluid must therefore increase from zero to its full value V_{str}. The region of fluid in which the velocity increases is called the <u>boundary-layer</u>. At increasing distances down stream from the leading edge of the flat surface, the fluid stream loses a greater total of momentum through the drag of the surface; and consequently more fluid is retarded. The boundary layer thus becomes thicker [16]. As the boundary layer merges into the main flow there is no sharp-line dermacation but for convenience the thickness of the layer may be taken as the distance from the surface at which the velocity reaches 99 percent of the velocity of the mainstream. The flow in the first part of the boundary layer is entirely <u>laminar</u> with increasing thickness, however, the laminar layer becômes unstable and the motion within it becomes disturbed. The irregularities of the flow develop into turbulence and hence the thickness of the layer increases rapidly. The random secondary moments of the turbulent flow die out very close to the surface and beneath the turbulent layer an even thinner viscous

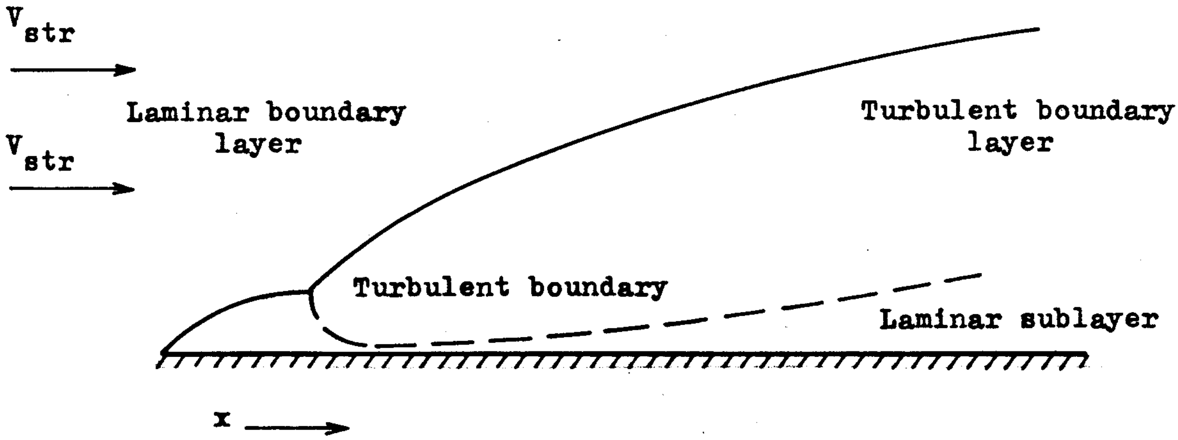

Fig. 6 Graphical representation of the boundary layer

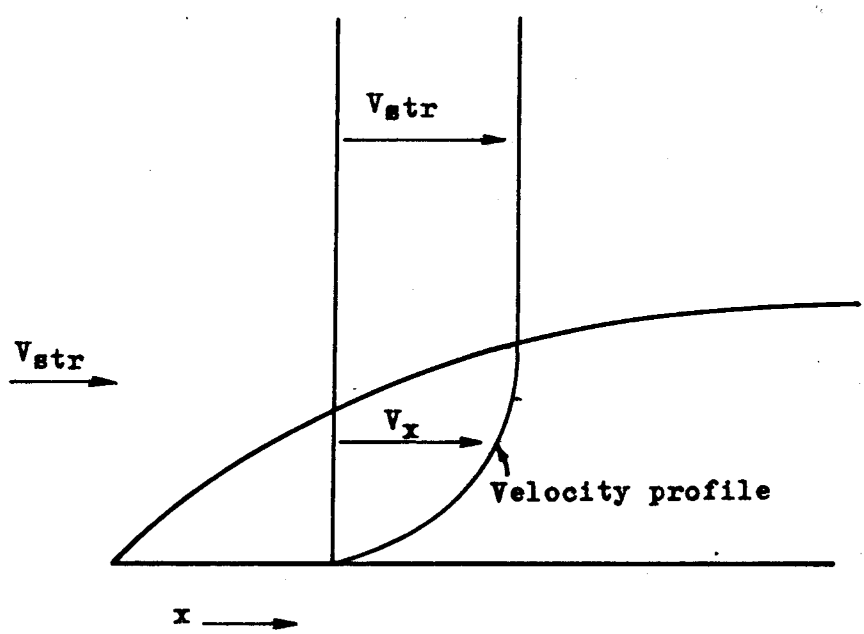

Fig. 7 Velocity profile for the boundary layer

sublayer is formed.

The hydrodynamic boundary conditions are given by the distribution of velocities at the nozzle exit and at the surface of the flat plate. However, the assumption that the surface is nearly at rest is never met in practical applications.

Graphical representation of the form of the boundary layer which develops when an incident stream of fluid velocity V_{str} impinges on a flat, smooth plate is given in Fig. 6. The velocity profile for the boundary layer is given in Fig. 7.

3.0 TRANSFER OF MASS WITHIN FLUIDS

Considering a system where a fluid flows over a flat surface and species diffusing from the plate to the stream, the basic equation defining the mass transfer rate k_m is,[16]

$$j = \frac{1}{A}\frac{dn}{dt} = -k_m \Delta C \qquad (40)$$

Therefore

$$\dot{n} = \frac{dn}{dt} = -k_m \; A \, \Delta C \; \text{(moles/sec)} \qquad (41)$$

The minus sign allows for the fact that $\frac{dn}{dt}$ is positive in the direction of decreasing concentration.

The equation gives the relation of the local mass transfer rate to the concentration gradient.

In turbulent systems, k_m is in some way related to the Schmidt number Sc,

$$Sc = \frac{\nu}{D} = \frac{\mu}{\rho} \frac{1}{D} \tag{42}$$

and directly dependent on the Eddy diffusivity given as

$$\frac{1}{A}\frac{dn}{dt} = - k_m \Delta C = -D_E \frac{d\bar{c}}{dy} \tag{43}$$

4.0 MASS TRANSFER IN A LAMINAR BOUNDARY LAYER WITHOUT CHEMICAL REACTION

(Derivation of the Mass Transfer equation)

If we assume that there is laminar flow [17] and

1) Low mass transfer rates,
2) constant physical properties past a solid surface,
3) mass transfer without reaction,

For an incompressible fluid, and two dimensional flow in the boundary layer, the equation of continuity is expressed as

$$\frac{\partial u_x}{\partial x} + \frac{\partial u_y}{\partial y} = 0 \tag{44}$$

The equation of motion is given as

$$u_x \frac{\partial u_x}{\partial x} + u_y \frac{\partial u_y}{\partial y} = \frac{\mu}{\rho} \frac{\partial^2 u_x}{\partial y^2} \tag{45}$$

If we have the diffusing species as A, the conservation of this species is expressed as

$$u_x \frac{\partial c_A}{\partial x} + u_y \frac{\partial c_A}{\partial y} = D \frac{\partial^2 c_A}{\partial y^2} \qquad (46a)$$

The equation can be expressed simply as,

$$u_x \frac{\partial c}{\partial x} + u_y \frac{\partial c}{\partial y} = D \frac{\partial^2 c_2}{\partial y^2} \qquad (46b)$$

Subscripts x, y denote velocity in x, y direction.

The above equation is arrived at by also assuming that

4) flow is two dimensional

5) diffusion in x-direction is negligible in comparison with the transfer of mass by the flow of the fluid.

The boundary conditions being

$u_x = u_y = 0$ at $y = 0$

$u_x = 0$ at $y = \infty$

$C = C_o$ at $y = 0$

$C = C_b$ at $y = y_\infty$

The above is the general mass transfer equation and its solution can yield the concentration profiles of the diffusing species in a system.

5.0 TURBULENT RECIRCULATING FLOW IN GAS INJECTED SYSTEMS

5.1 Introduction

In all gas injected systems used in Metallurgical practice, gas bubble stirring provides effective agitation although both the turbulent motion induced and the velocity fields are quite strongly non-uniform.

5.2 The Recirculating Flow

One key feature of gas injection at atmospheric pressure is that it provides effective convective mixing in order to

- homogenise the melt
- provide oxidation and reduction i.e. refining.

In an agitated refining unit, a turbulent recirculating flow exists and the materials in the system may be dispersed by two mechanisms, namely

- bulk flow i.e. motion of the bath
- eddy or turbulent diffusion

The bulk motion of the fluid will be responsible for carrying the materials along the 'existing' streamlines (which defines the circulation pattern), while eddy diffusion, which acts in all directions will be primarily responsible for transporting materials across the streamlines. These two infact have to act together, in order to promote mixing. If the flow is laminar, very little mixing is possible.

The role of convective mixing is extremely important in the mentioned operation in addition to controlling the rate of homogenisation and dispersion of additions. Mixing also plays a vital role in transporting the reactants to the reaction zone for example, in oxidation and desulphurisation [27].

The terms on the right side of equation (41)

$$\dot{n} = -k_m A \Delta C \tag{41}$$

could be assumed to represent eddy or turbulent diffusion and convective transport due to bulk flow. It should be emphasised that the term k_m is very much related to the nature of flow. To some extent, the turbulent kinetic energy or turbulent energy dissipated in a system plays a key role in determining the transport coefficient.

In gas stirred units a gas plume or bubble exists and because of its reduced density, provides a recirculating flow pattern. Since the flow is driven by the density deficit, the precise knowledge of the bubble shape is desirable for accurate representation of the system.

Turbulent characteristics, velocity field, heat transfer, mass transfer and fluid flow phenomena in turbulent recirculating flows can be determined by utilising the Navier-Stokes equations and using the appropriate boundary conditions, although in general this would be done through the equation of motion because of restrictions in the Navier-Stokes equations.

6.0 FLOW PAST A SOLID SURFACE

If we consider a fluid flowing past a solid surface, either in the laminar or turbulent regime at the same time assuming that all resistance to mass transfer is confined to a stagnant layer of thickness adjacent to the surface;

The molar flux of diffusing species A is given as

$$N_A = - D_{AB} \left(\frac{\partial C_A}{\partial z} \right)_{Z=O} = -C\, D_{AB} \frac{\partial x_A}{\partial z} \qquad (47)$$

This is the Fick's law for the Z-direction.

D is characteristic of a constituent and its environment [17].

The above equation is also written as

$$N_A = - D_{AB} \frac{\partial C_A}{\partial z} = k_d \, (C_{Ai} - C_{Ao}) \qquad (48)$$

and is mostly used in cases of molecular diffusion in fluids.

For the case of a stagnant layer of thickness adjacent to the surface, in terms of x.

$$N_{A,y} = \frac{C\, D_{AB}}{\delta} \quad \frac{(X_{Ao} - X_{A,b})}{(X_B)\ lm} \tag{49}$$

In terms of molar concentration,

$$N_{A,y} = \frac{C\,D_{AB}}{\delta} \times \frac{(C_{Ao} - C_{A,b})}{(C_B)\ lm} \tag{50}$$

Equating (49) and (50)

$$k_d = \frac{C\, D_{AB}}{\delta\,(C_B)\ lm} \tag{51}$$

for the case where C_{Ao}, $C_{Ab} << C$ i.e. at low concentration of diffusing species A, we have

$$(C_B)\ lm \equiv C$$

Therefore

$$k_d = \frac{D_{AB}}{\delta} \tag{52}$$

This gives

$$N_{A,y} = \frac{D_{AB}}{\delta} (C_{Ao} - C_{A,b}) \tag{53}$$

The thickness of the film δ for fluid flow past a surface in forced convection differs for turbulent and laminar flow regimes and it has been found that the local mass transfer rate is much less position dependent in turbulent flow.

6.1.0 ALTERNATIVE THEORIES OF MASS-TRANSFER AT FLUID SURFACES

6.1.1 Introduction

A number of theories have been developed which show that the assumption of a stagnant film is an idealization of a fairly complex flow situation as given in the preceding paragraphs.

6.1.2 THE SURFACE RENEWAL THEORY-HIGBIE THEORY

The theory postulates that a fluid element comes in contact with the surface for a certain period of time, during which unsteady state diffusion occurs between the fluid element and the surface. At the end of this time period, the fluid element is swept away from the surface and replaced by a new element from the bulk.

Equations have been developed from this theory on the assumption that the contact time is so short that the concentration gradient in the element between the surface and the fluid element, the latter may be regarded as semi-infinite in thickness, this means that the contact time is so short that the concentration gradient in the element does not penetrate to the side of the element away from the surface.

For low concentration of diffusing species, the diffusion equation in the fluid element is,

$$\frac{\partial c_A}{\partial t} = D_{AB} \frac{\partial^2 c_A}{\partial y^2} \tag{54}$$

For $0 \leq y \leq \infty$ and $0 \leq t \leq t_e$

t_e = contact time i.e. the residence time of fluid element at the surface.

The molar flux of A crossing the y = 0 plane is expressed as

$$N_A = - D_{AB}\left(\frac{\partial C_A}{\partial y}\right)_{y=o} = (C_{A,o} - C_{A,b})\left(\frac{D_{AB}}{\pi t}\right)^{\frac{1}{2}} \quad (55)$$

For low concentration of diffusing substances,

$$k_d = 2\left(\frac{D_{AB}}{\pi t_e}\right)^{\frac{1}{2}} \quad (56)$$

which shows that

$$k_d \propto D_{AB}^{\frac{1}{2}} \quad (57)$$

The Film theory; $k \propto D_{AB}$ and the Penetration theory $k \propto D_{AB}^{\frac{1}{2}}$ assume the surface elements to be essentially deep, the diffusing species never reaching the region of constant concentration below.

The observed dependence $k \propto D_{AB}^{n}$ with n dependent upon circustances, might be explained by allowing for a finite depth of the surface elements or eddies.

6.1.3 THE SURFACE-STRETCH THEORY

Lightfoot and Co-workers [21] have extended the penetration surface-renewal concepts to situations where the interfacial surface through which mass transfer occurs changes periodically with time, which happens to be the case in the present work.

If the flow is thoroughly turbulent, the mass transfer resistance will reside in a surface of varying thickness. This situation occurs at nozzles and when the liquid surfaces are wavy [17].

In the present case of gas bubbling in a submerged tuyere, when the bubbles form to their maximum size at the surface of the tuyere, they influence the fluid flow at the surface in a fashion where the fluid flow in the wall region fluctuates in a right to left manner thereby affecting the character of mass transfer as such the mass transfer rate will also be dependent on this behaviour.

6.1.4 THE WALL REGION

The flow in this region can be divided into two sublayers i.e.

1) Inner layer, where the flow is influenced by the wall.
2) Outer layer, where the flow is influenced by the surrounding fluid.

6.2 The Schmidt Number, Sc

In turbulent flow with mass transfer, there is still a thin laminar sub-layer of thickness δ_h close to the flat solid surface which results from viscous drag and if mass transport is occuring at the surface there will also be a diffusional boundary layer of thickness δd.

The relationship between the thickness δh and δd is governed by the dimensionless Schmidt Number Sc.

$$S_c = \frac{\nu}{D} = \frac{\mu}{\rho D} \qquad (42)$$

The higher S_c is, the thinner will be the diffusion layer and the more rapid will be its formation. If both δd and δh start to develop together then

$$\frac{\delta h}{\delta d} \geqq S_c^{\frac{1}{2}} \qquad (58)$$

6.3 Turbulent Flow

In turbulent flow, transfer of momentum between neighbouring pulses of the fluid are of primary importance. These inertial (momentum) effects in turbulent flow (as contrasted with purely viscous effects in laminar flow) cause the velocity and density of the flowing fluid to assume great importance [16]. Turbulent flow replaces laminar flow when these inertial effects are great compared with viscous effects.

Near the surface of a flat plate, the strong velocity gradient within the fluid shears the fluid into small eddies. Some of these migrate towards the bulk of the flow where larger eddies are also found.

Even in turbulent flow, a laminar sublayer exists near the surface. Beyond the laminar sublayer, turbulent flow exists. For a flat plate, at low relative velocities between plate and solution, flow is laminar and at high velocities it is turbulent. Transition occurs over a velocity range and depends on

a) Geometry

b) Viscosity of the liquid and

c) roughness of the surface

In the derivation of differential equations, turbulent flows can be treated as though they were steady laminar ones, with the transport properties varying in magnitude from place to place in the flow[19].

7.0 MASS-TRANSFER COEFFICIENT

The nature of transfer of dissolved substance through the fluid will depend upon the nature of the fluid motion prevailing in various regimes.

The overall transport of mass consists of bulk convection and turbulent convection. With the bulk convection there is a net transport of fluid involved. With the turbulent convection there is an exchange of fluid between the boundary layer and the bulk. Both bulk convection and turbulent convection depend on the driving force; bulk convection on diffusivity D, while turbulent convection is a function of the eddy diffusivity D_E.

The overall resistance to mass transfer is empirically found by defining the mass transfer coefficient K as

$$K = \frac{\text{rate of mass transfer}}{\text{concentration driving force}} \qquad (59)$$

where strictly speaking, the driving force is the difference in chemical potential.

For the determination of Mass transfer coefficient, a great reliance is put upon experimental measurements.

8.0 SOME FACTORS AFFECTING MASS TRANSFER AND MASS TRANSFER COEFFICIENT

1) Mass flowrate
2) The kind of component transported
3) Geometry i.e. size and position of the nozzle relative to solid surface.

4) The hydrodynamic conditions as mentioned above e.g. distribution of velocities. Sometimes these could be kept constant.

The influence of turbulence level at the nozzle exit which is never taken into account in the design equations should also be taken into account.[20]

Liquid film on inside wall
with gas in centre

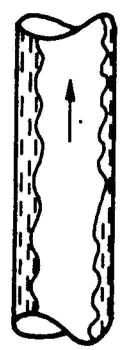

Fig. 8 **Flow pattern of upward vertical annular flow**

The two-phase flow is reviewed because the flooding characteristics have a relation to inner pipe or tuyere erosion in steady flow.

1.2 The Annular Vertical flow pattern

Upward vertical flow of liquids in tuyeres or pipes is mainly divided into four categories; Bubble flow, slug flow, churn flow and Annular. In the present work, we have annular flow only. The annular vertical flow pattern is characterised by an upward moving continuous smooth to wavy film of the liquid on the tuyere wall and much more rapidly moving central core of gas, containing, at times, entrained droplets of liquid in a concentration which may be wholly in laminar motion or it may be laminar only nearest to the wall, and turbulent nearest the gas-liquid interface. The gas-phase is in turbulent motion and at steady-state [22].

At any given liquid rate, decreasing the gas rate causes more of the liquid to be present in the film, the liquid film velocity to decrease and its thickness to increase. At a certain critical gas rate the liquid film velocity decreases to zero, and below this rate the film thickens rapidly, has a negative velocity near the wall, penetrates the gas-phase and froth flow occurs.

For any given fluid system, the major factors in determining the flow patterns are the flow velocities. The lack of knowledge of the velocities at a point in the individual phases makes it impossible to give any real picture of the velocity distribution. In most cases the gas-phase which may be flowing with a much greater velocity than the liquid, continuously accelerates the liquid. (For cases where the flow of both phases is co-current). This involves a transfer of energy. Either phase may be in streamline or in turbulent flow, but the most important case is that in which both phases are turbulent. The criterion of streamline or turbulent flow depends on the Reynolds number [22]. This distribution is to some extent arbitrary in that injection of a gas into a liquid initially in streamline flow may result in turbulence developing.

The more important factors in two-phase flow which a designer must seek to understand and be able to evaluate are the stability of flow, the likelihood of the flow causing erosion problems, the relative volumes of the two-phases present in the pipe or tuyere and the pressure drop caused by the presence of an additional phase.

1.3 Erosion in Multiphase Flow[23]

Two-phase systems in steady pipe flow, are often accompanied by erosion, and many empirical relations have been suggested to avoid the condition. Since high velocities may be desirable to avoid the instability associated with flooding of the tuyere, there is a danger that any increase in the through-put above the normal operating conditions will lead to a situation where erosion may become a serious possibility.

1.4 Some Fundamental concepts of two-phase flow

To some extent, equations have been developed for describing the two-phase or multiphase systems by considering that adsorption and surface tension effects are negligible. The application of these fundamental equations of flow to multiphase flow have been complicated by the following factors:[22]

1) The flow of multiphase mixtures may not be characterised as laminar, or as a combination of laminar and turbulent flow but relative quantities and distribution of phases (i.e flow pattern) must be considered.

2) Because of the differences in phase densities and frictional effects the flow pattern in the vertical flow is not symmetrical about the flow axis.

3) Presence of the interface between the phases adds problems as equations must be written for it as well.

4) In most cases, the separate phases move at different average velocity and the in-situ concentrations are not the same as the concentrations in which the phases are introduced.

2.0 TUYERE EROSION

2.1 The Contact radius, r_c

It has been suggested[3], that the lateral movement of the gas-liquid interface across the surface surrounding the tuyere mouth during the bubble growth could lead to erosion of the tuyere. During the formation of discrete bubbles and the large stems, the hydrodynamical interaction between the fluid phase and the vessel wall could influence the erosion in commercial vessels. The variation of the contact radius[12], r_c is such that it is a maximum during the initial growth of the bubble, when the wake of the preceding retracting stem has little influence on the forming bubble. The contact radius can be defined as

$$r_c = \frac{d_b}{2}$$

d_b = diameter of bubble base in contact with surfaces surrounding the tuyere.

2.2 Bubble Regimes

On supposing that tuyere mouth erosion is related to sweeping behaviour, it is evident that the Three Bubbling regimes (coalescence regimes) would give markedly different erosion profiles. The nature of the Bubbling regimes is also explained in section 1.2 of Chapter 1.

1) Stem formation with binary coalescence would produce a reasonably uniform erosion profile across the whole contact area.
2) Erosion during orifice coalescence regime would be concentrated near the tuyere mouth,

and

3) Stem coalescence would produce an erosion effect somewhere in between the two extremes.

The gas flowrate also affects the tuyere in erosion in that, at increased flowrate, gas momentum effects play an increasingly important part in determining the shape and volume of discrete bubbles, formed at the tuyere.

The 'Blowing back' (Back Attack) of the jet which attacks the tuyere front has also been suggested as being one of the reasons of tuyere erosion. This is said to occur when the bubble constricts at the point close to the tuyere on detachment. This is said to develop and sweep away with a downward flow [8].

2.3 'Back-Attack' Phenomena [8]

It has been suggested that when a jet is blown into water it is found that the jet blows back onto the front surface of the tuyere. This cavity is constricted and a large bubble is formed. This phenomena occurs at a significant frequency. The front surface of the tuyere receives an impact at the moment the jet blows back.

Water penetrates the cavity at a distance of twice that of the tuyere diameter, from the tuyere's tip, then passes down stream.

A representation of this behaviour is given in Fig. 9.

It has been suggested[9] that the effect weakens as erosion proceeds. The decrease in V_o in this case may encourage freezing and accretions. The sweep cycle can be eliminated by high momentum force F_M, and Injection Number, N_I.

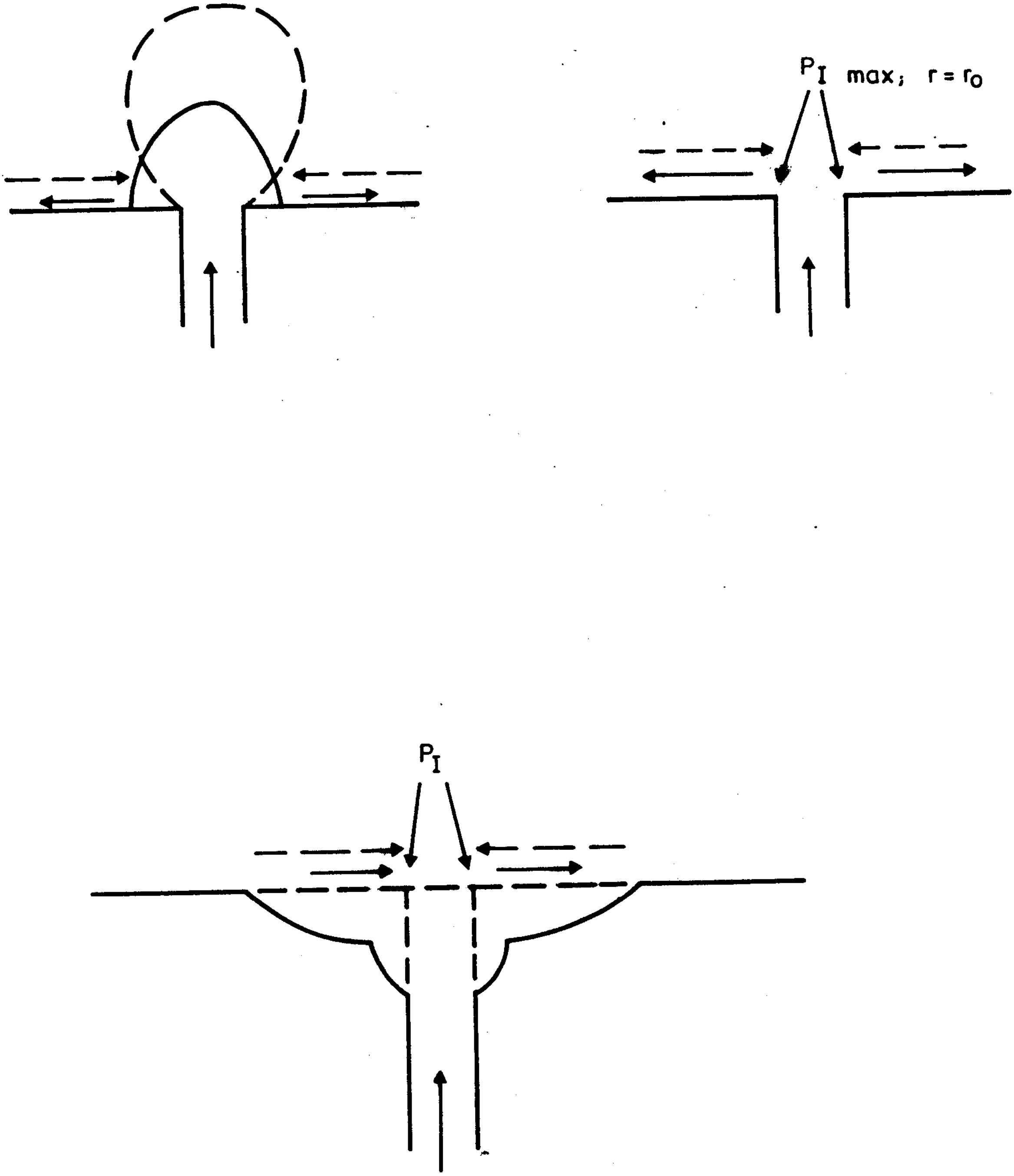

Fig. 9 **Nozzle mouth pressure impulse "Back Attack"**

Experimental techniques used by Boxall et al [10] show that freezing, i.e knurdle formation and growth, is possible.

Collins [11] using Air/Water models found that one of the mechanisms contributing to tuyere wear is the running of the liquid into the tuyere. Experiments showed that the wetting strongly depended on the

a) Gas flowrate

and b) Tuyere diameter.

Experimental findings agree well with pilot plant operations.

From the foregoing literature, the mechanism of bubble/growth, wall interaction and parameters influencing the bubble formation will be observed to explain the nature of tuyere erosion and the effect various parameters have. Based on equations (40) and (41), the mass transfer mechanism will be studied.

Two phase flow will be studied to see to what extent the liquid entrainment influences the erosion profile.

The acceptable range of Modified Froude Number and Injection Number as applies to commercial operations will also be observed.

CHAPTER FOUR

1.0 EXPERIMENTAL METHODS AND RESULTS

1.1.0 PREPARATIONS

1.1.1 TUYERE MODEL (PLASTER)

The soluble tuyere panels used in determining the erosion mechanism, were made of surgical plaster of stoichiometric composition $(CaSO_4)_2.H_2O$. The plaster blocks were cast in plastic containers by mixing with water. Since the strength, setting time and porosity of the plaster casts depends much on the water to plaster ratio (water/plaster), different water/plaster ratios were cast and it was found that a plaster mix of 1:2 water to plaster ratio gave a reasonable setting time of approximately 5 minutes, good porosity and strength similar to that of tuyeres used in commercial practice. This was based on similar work carried out by other workers. (28) The blocks of plaster were then placed in Hydrochloric acid (HCl) of varying strength in the range of 0.4M to 0.6M HCl and agitated to determine the extent of acid attack on the blocks as the rate of erosion of the plaster depended on the acid strength. It was found that the acid strength of 0.45M gave a reasonable rate[28] for plaster of 0.5 water/plaster ratio.

The plaster blocks or tuyere panels were machined with care to make the half- slice tuyere panels of dimension 8.6 cm diameter and 2.4 cm depth. The tuyere diameters drilled were 3.0, 4.0 and 5.0 mm for the Helium - Hydrochloric acid experiments and 6.0 mm for the Air-water experiments. To avoid acid attack on the other surfaces not important to the work, the surfaces were vanished.

Half slice models were used so that bubble growth behaviour, tuyere erosion profile and two-phase flow characteristics could be monitored easily.

1.2 GENERAL DESCRIPTION AND PROCEDURE

1.2.1 APPARATUS

The main equipment used consisted of a perspex tank of dimensions 27.5 cm square and 82 cm deep. For the present work, at all times experiments were carried out at a seal depth of approximately 30 cm from the bottom of the tank. A 'dummy' wall which held the tuyere block was mounted firmly to the inside of the tank's front surface. A Schematic drawing of the apparatus is shown in Fig. 10. The tuyere blocks were placed about 9 cm

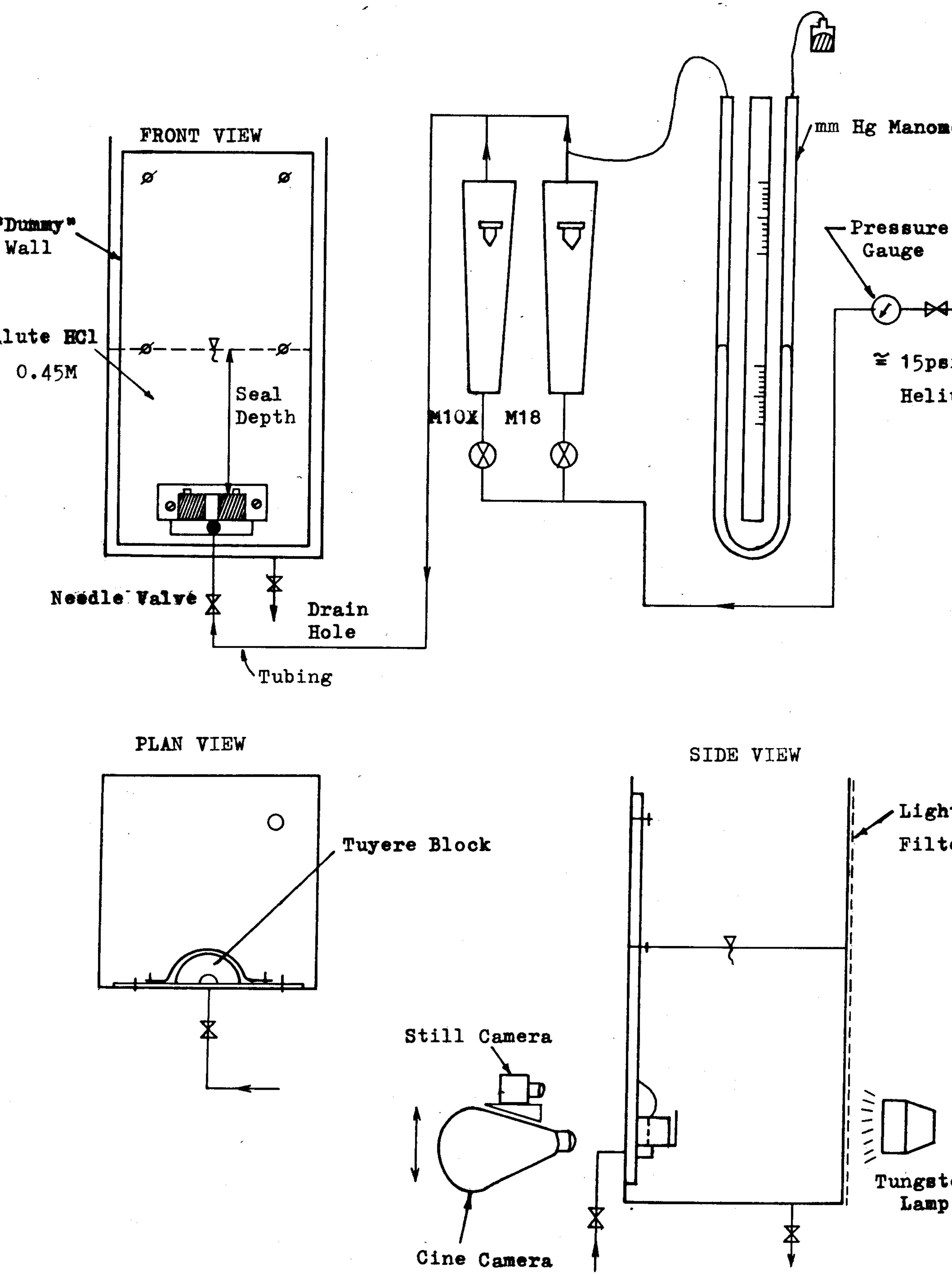

Fig. 10 Schematic diagram of experimental apparatus

above the base of the tank and connected to a needle valve which controlled the gas supply. The valve was connected as closely as possible to the tuyere to achieve a constant gas supply, it was connected using a 1 inch bore pipe. In this case the effect of fluctuations in flow due to sub-nozzle volume could be neglected[24,25,26]. An ideal tuyere would appear as given in Figures 9&. The gas supply system between the control valve and the supply valve had two flowmeters which were calibrated for measuring the flowrates of the gases used and a mercury manometer for measuring Atmospheric pressure. The supply pressure was maintained at approximately 15 psi Air and Helium.

A 16 mm high speed stalex cine-camera operating at 200 to 250 frames/sec was used in monitoring the bubbling behaviour and the two-phase flow characteristics. A still camera was also used.

For measuring the concentration of calcium in the bath of acid at particular time intervals of blow, the use of the Atomic Absorption Spectrophotometer was employed. Calibration of the AA spectrophotometer was done by preparing a 0.1% Ca solution of Calcium chloride (CaCl) from $CaCO_3$ and HCl as standard which was diluted to various concentrations. To determine ΔC in the equations (40) and (41) where $\Delta C = C_{sat} - C_{eq}$, C_{sat} was found by crushing the plaster blocks and then dissolving in 0.45M HCl to form a saturated solution which was filtered for precipitates and the filtrate solution was left to cool overnight before analysing for C_{sat}. The obtained value of C_{sat} was 1.77 grams/litre i.e 1.77×10^{-3} grams/ml (6.1 moles/m^3) which was much higher than the $C_{eq} = 1.0 \times 10^{-4}$ g/ml as such ΔC was taken as $\Delta C \simeq 1.77$ g/l.

The determination of parameters affecting tuyere erosion was studied by using a Helium - Hydrochloric acid system (He/HCl) at ambient temperature. Prior to this an Air-HCl system for economic reasons was used to determine the time of operation when a reasonable rate of erosion occurred and other experimental conditions.

It was decided from the Air/HCl preliminary experiments to have each experiment running for 30 minutes. In this 30 minutes, appreciable erosion could occur and 20 ml samples of the acid in the tank were taken at intervals of 10 minutes to determine the trend of erosion, and at the sametime, still and cine-photos were taken to determine the extent of erosion, the effect of bubble growth, in particular the maximum attainable horizontal bubble radius r_c on erosion and diameter of tuyere at 10, 20 and 30 minutes i.e d_{10}, d_{20} and d_F. Tuyere blocks were also weighed before and after use as a second check to weight loss due to erosion. Plate 1 shows the still photos of the erosion profile. Plate 2 shows the bubble formation sequence and variation of r_c.

The effect of the two-phase flow in the tuyere was studied by using an Air-Water system. The water was coloured using a blue water soluble dye for easy visual perception. The dye was such that it did not appreciably affect the viscosity and flow characteristics of the water. Colour cine-films of the annular flow pattern were taken at 10 minute intervals for particular flowrates with a tuyere diameter of 6 mm. Fig 11 shows the trend of flow in the tuyere.

In all the experiments the cameras were placed close to the tank. Front lighting only was used for the two-phase flow observations while in determining the bubble behaviour, the lighting was at the back of the tank with a translucent filter placed in front of the light to avoid scatter and one lamp was at the

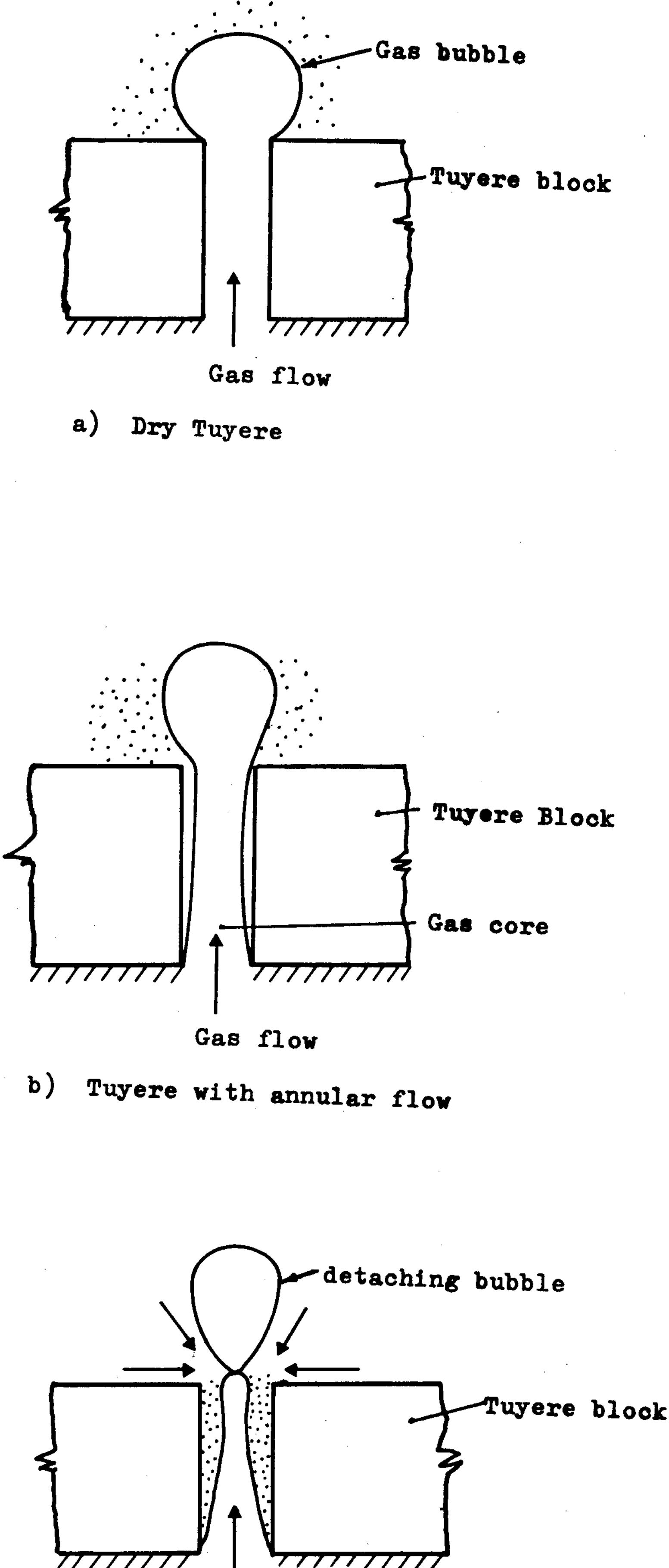

a) Dry Tuyere

b) Tuyere with annular flow

c) Flow at bubble detachment

Fig. 11 Tuyere with two-phase annular flow front face. The still camera was used to observe the extent of both lateral and axial erosion as seen in plate 1.

The following parameters were observed to fully explain the erosion mechanism as shown in Table 1 and 2.

1) The gas flowrate

2) The original tuyere diameter d_o (mm) and for / each particular flowrate Q,

3) The tuyere diameter after 30 minutes, d_F as well as the tuyere diameter after every 10 minutes from still photos and the blocks as a second check.

4) The maximum bubble radius attainable after every 10 minutes (by Cine film analysis on the film analyser) and the growth behaviour.

5) Weight loss of sample

6) Determining the ΔC, i.e ΔC which was found to be $\Delta C = 1.77 \times 10^{-3}$ g/ml or 6.1 moles/m^3.

The parameters observed during the two-phase flow were, as shown in Table 3.

1) The gas flowrate

2) The mean liquid film thickness δ (from cine film analysis).

3) The relative volume percent of the liquid in the tuyere.

1.3 FLOW CONDITIONS USED

Based on the theory that bubbling occurs in the Injection Number range 0.0 to 0.1. See Fig. 5 e.g. for copper converting it is 0.06, it was decided to operate in the injection number range of 0.05 to 0.06. A wider range of injection numbers was used for the two-phase flow experiments. See Table 3.

Three flowrates were chosen corresponding to the injection numbers 0.05, 0.055 and 0.06 for each particular orifice diameter. The Modified Froude Number N_{Fr}^* range for all the experiments was within the acceptable range of 10 to 200. See Tables 1, 2 and 3.

2.0 DISCUSSION OF RESULTS

2.1 Mass Transfer Study

In the plot of moles eroded against time shown in Figures 12 to 15, average values of repeated experiments are shown for tuyere diameters 3.0, 4.0 and 5.0 mm. The computed solutions of the given equations are corrected for the different diameters used. Using a standard Mathematical pack, a regression analysis of the data obtained was done to obtain the best fitting curves. The results of Figures 12 to 17 show that at different diameters, with increasing flow conditions of N_I = 0.05 to 0.06, the tuyere is eroded with increase in time of gas injection.

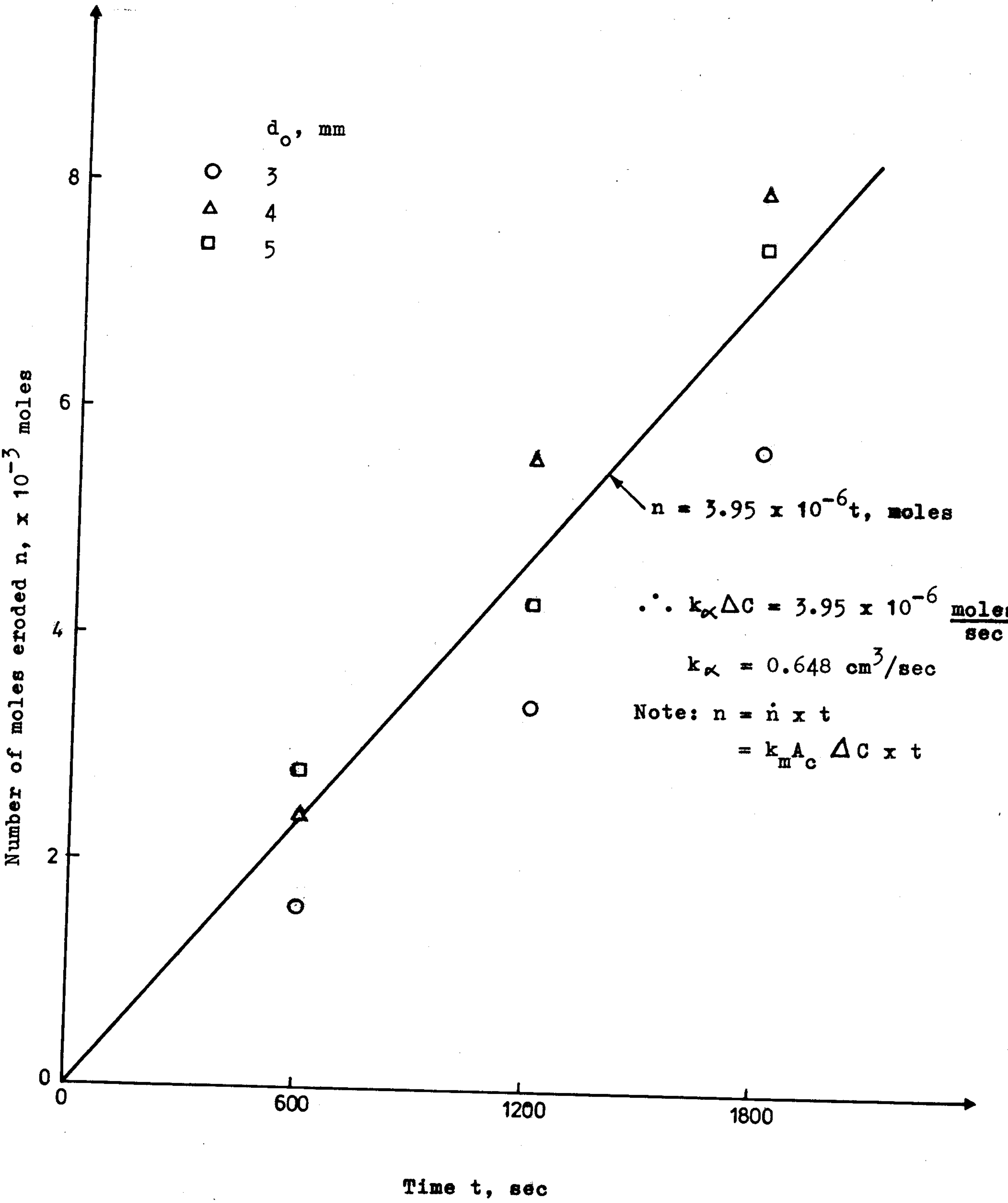

Fig. 12 Amount eroded with time at $N_I = 0.05$

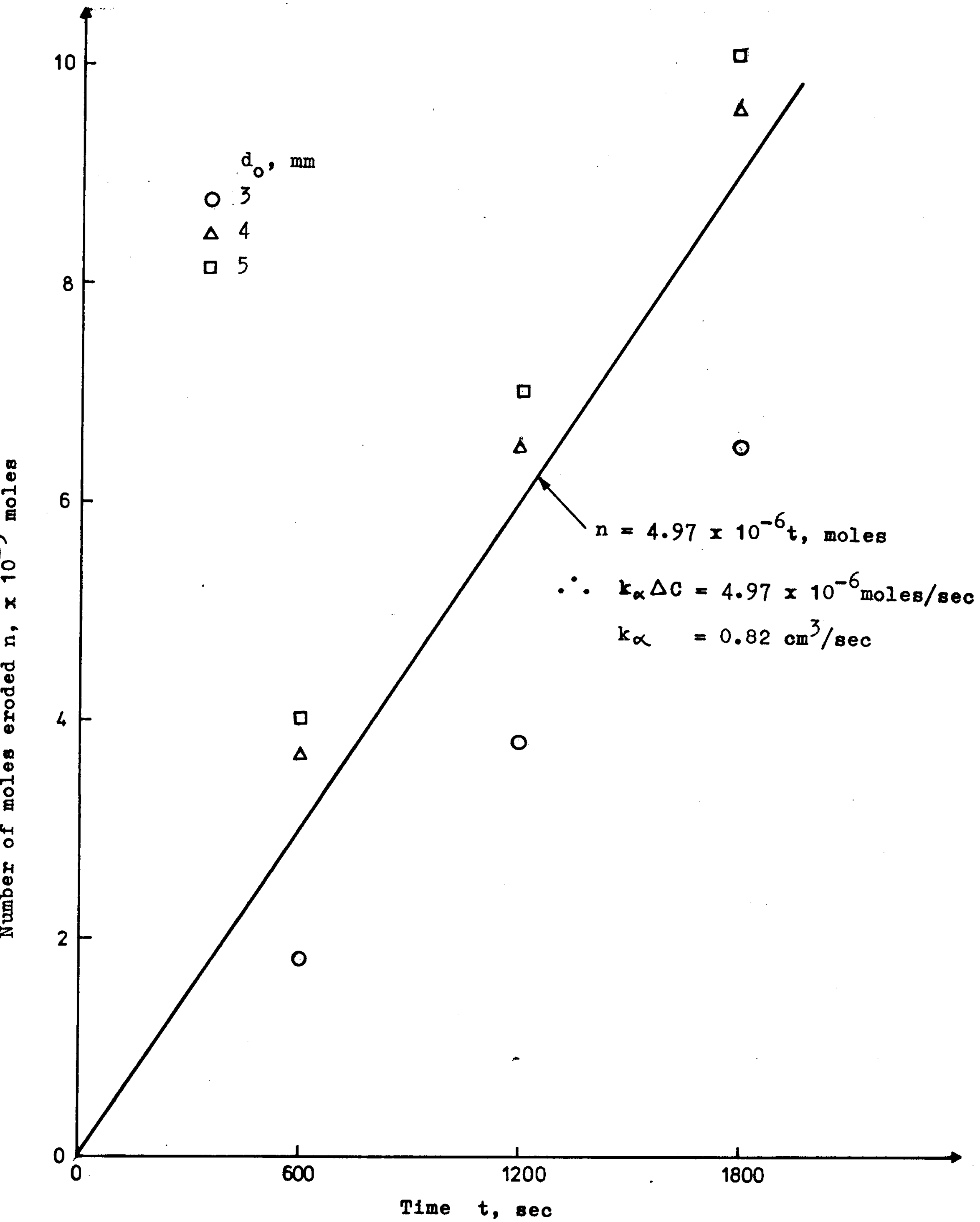

Fig. 13 Amount eroded with time at N_I = 0.055

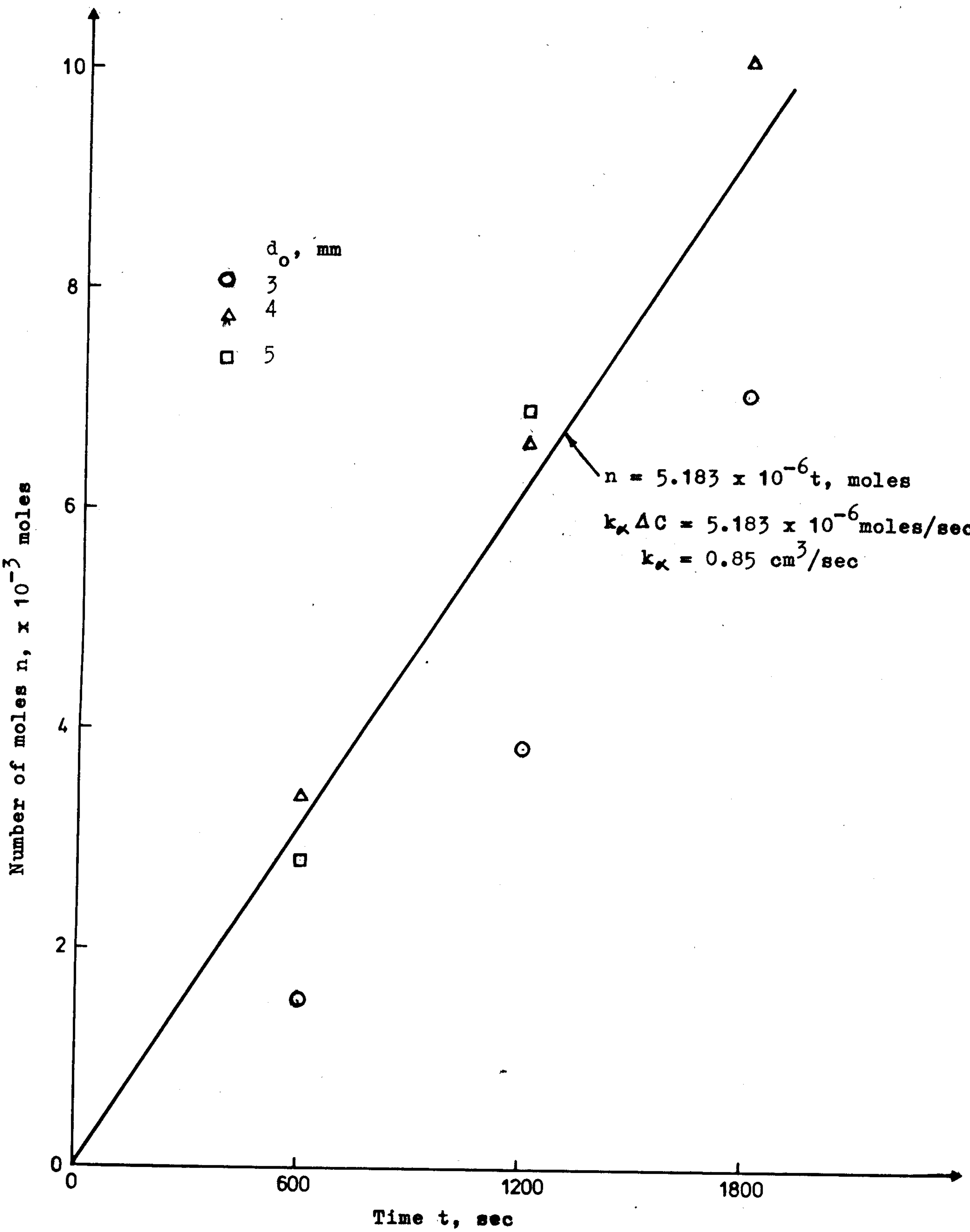

Fig. 14 Amount eroded with time at $N_I = 0.06$

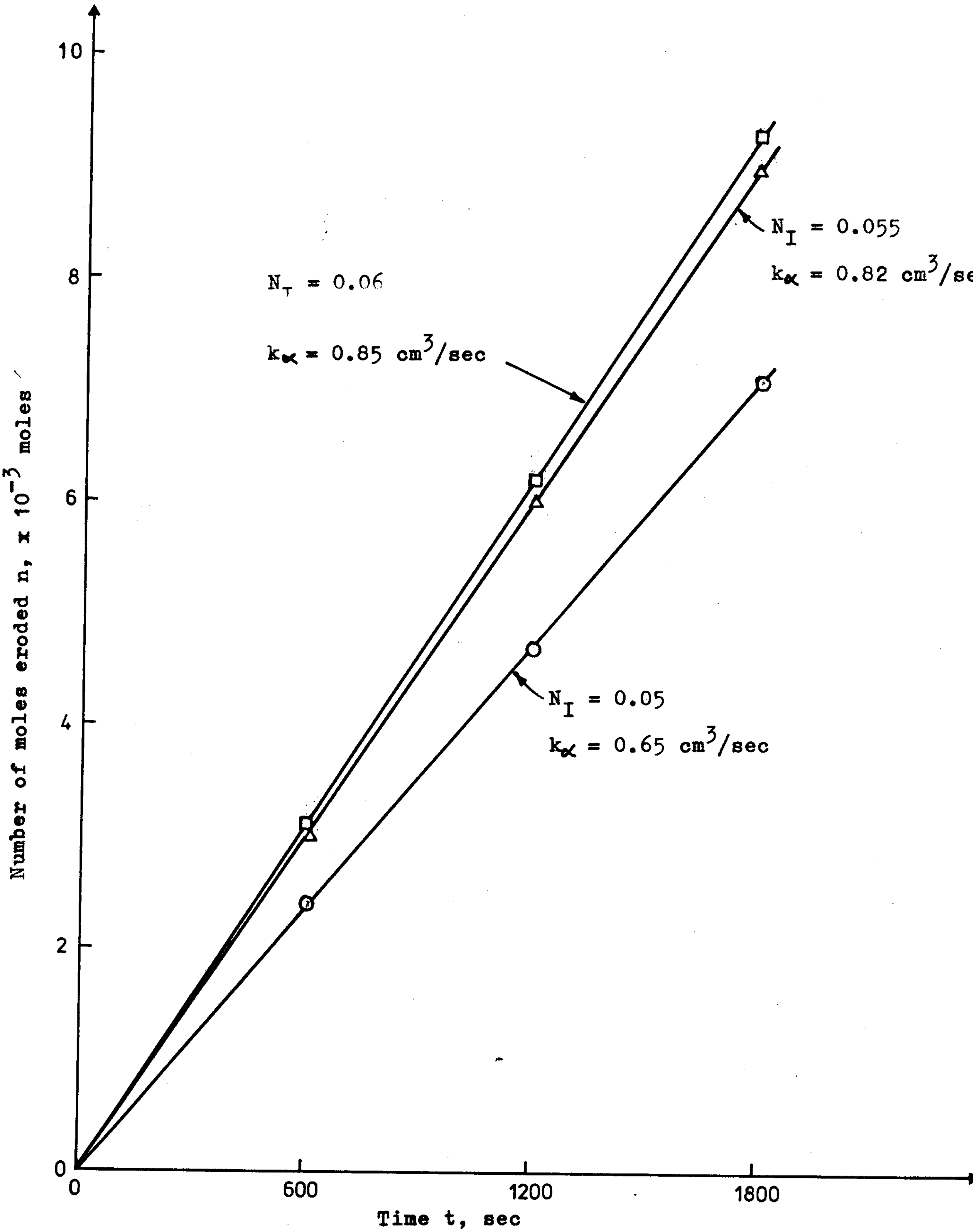

Fig. 15 Amount eroded with time at varying N_I

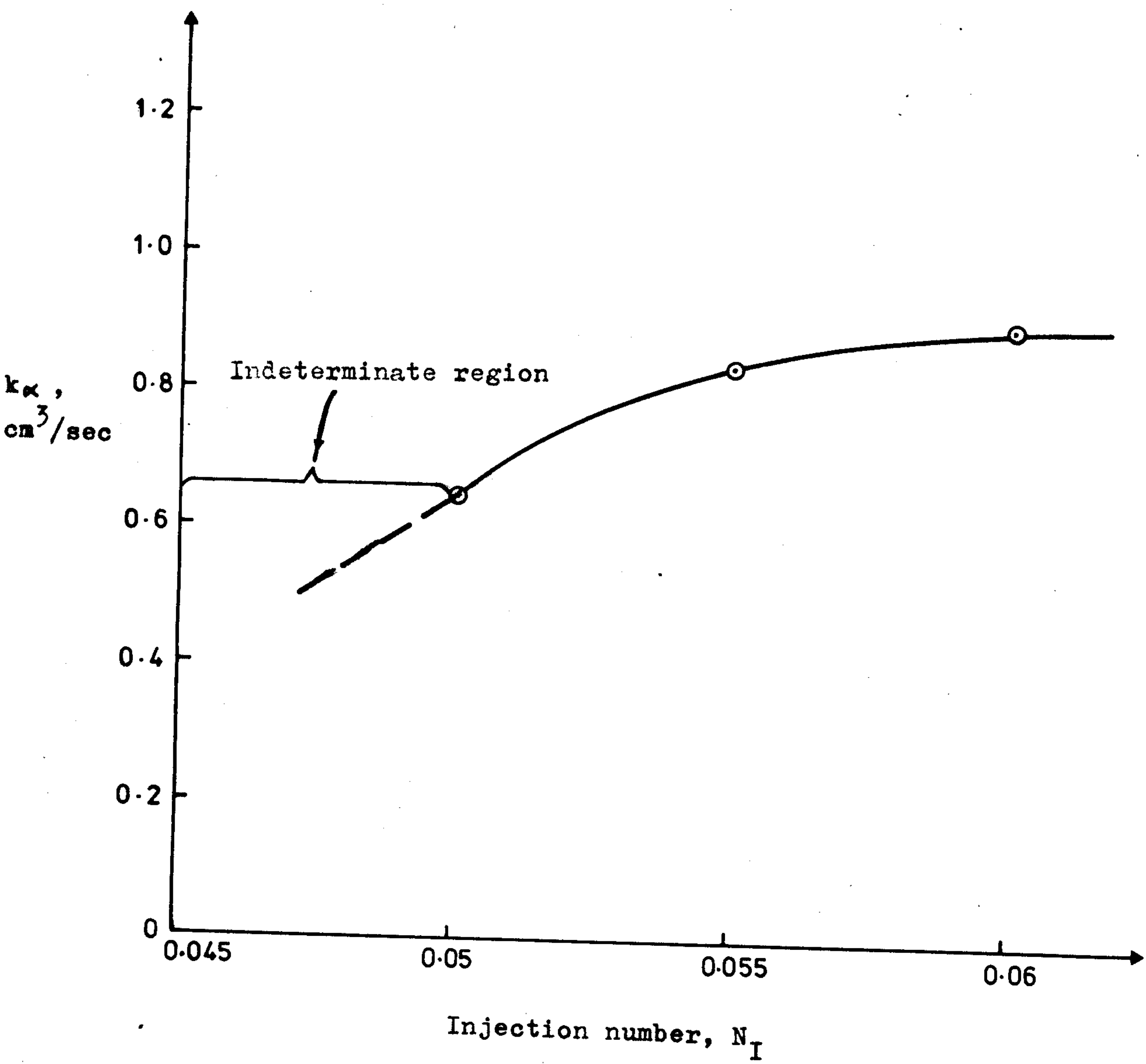

Fig. 16 Variation of k_α with injection number

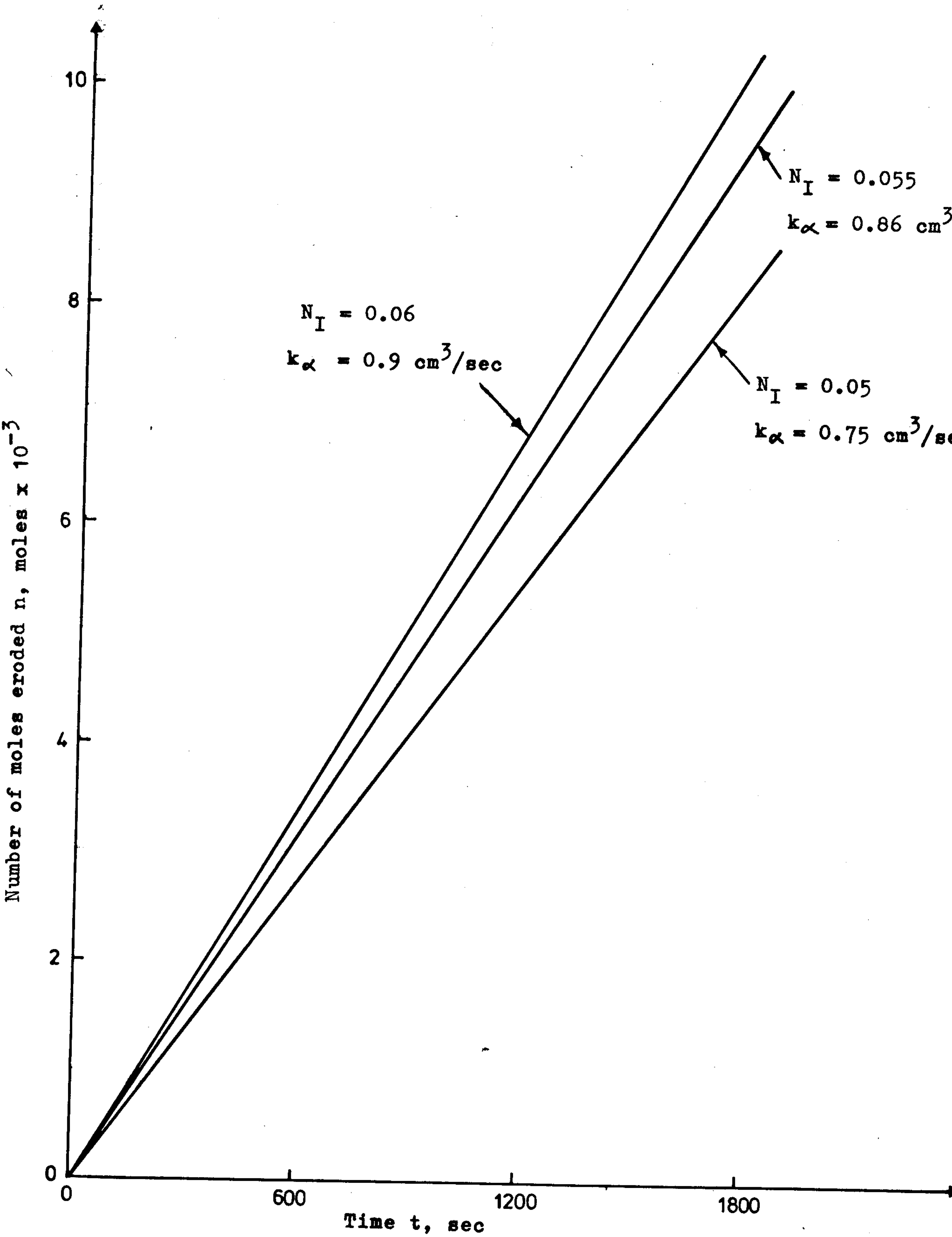

Fig. 17 Amount eroded with time at constant diameter (d_o=4mm) with varying flowrates, N_I

A value of $k_{\alpha} = k_m A$ is determined in this work to account for the flactuating nature of the flow due to bubble movement, washing effect and agitation on the tuyere surface, it is also assumed to account for the eddy nature and diffusivity of the system as a proper value of k is difficult to obtain under the recirculating flow conditions. From equation (41), the shape of the graphs for moles eroded against time is is given as

$$\text{Slope} = k_m A \Delta C = k_{\alpha} \Delta C$$

Since $\Delta C = 6.1$ moles/m^3 is known, k_{α} can be calculated from the obtained slope.

The Figures 15 and 16 show the trend that k_{α} increases with the injection number N_I at a particular tuyere diameter. For the situation in Metallurgical operations where $N_I \geqq 0.05$ to 0.06, the k_{α} values will be in the range of 0.65 to 0.85 cm^3/s.

A relation of final tuyere diameter d_F to the Froude Number N^*_{Fr} for various tuyere diameters has been found to be linear and equal to

$$d_F = 0.05\, N^*_{Fr} + d_o$$

at the same time, the increase in diameter with time is such that

$$d_{x,t} \cong 0.1t + d_o$$

were $d_{x,t}$ is the diameter at a given time. See Fig. 18 and Fig. 19.

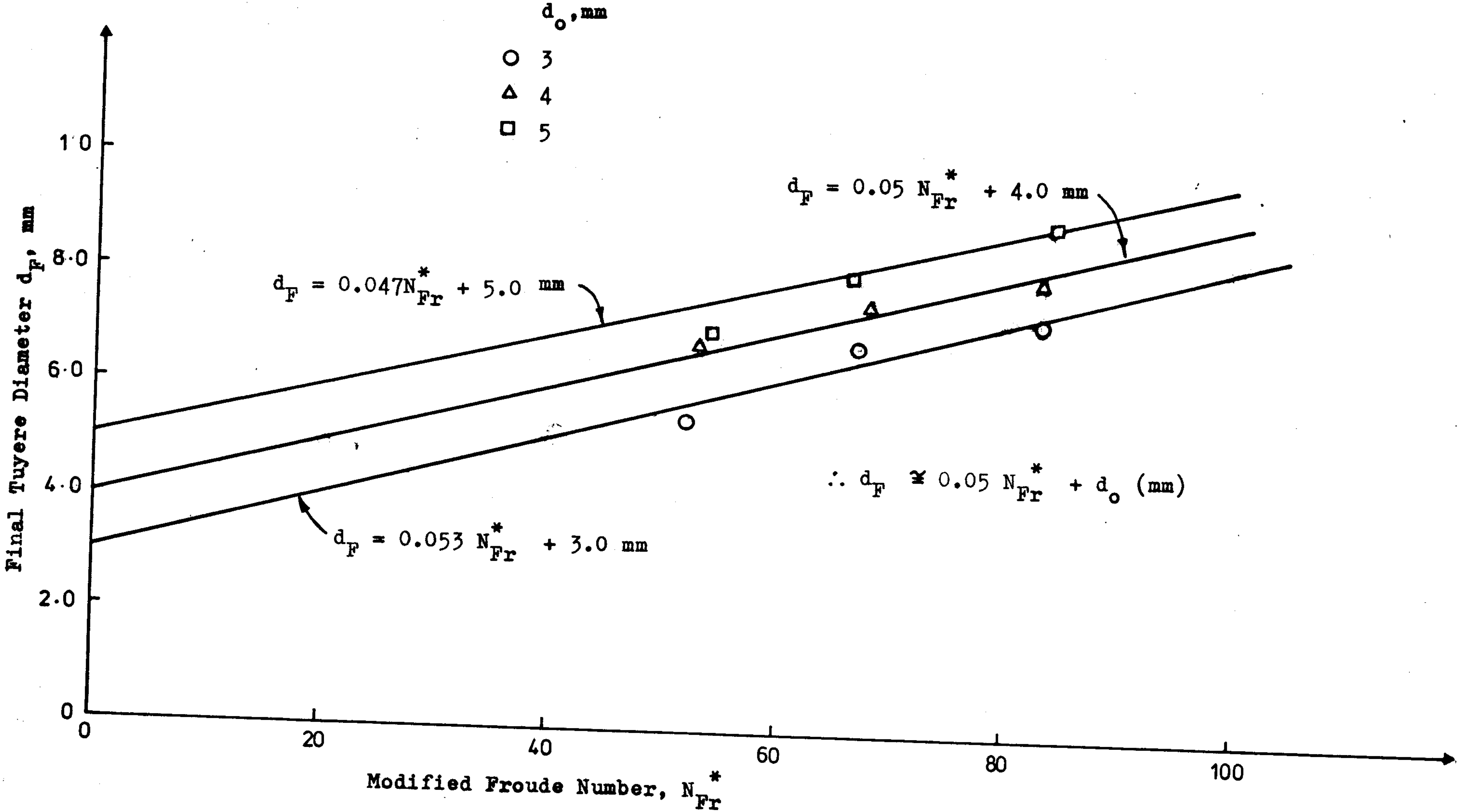

Fig. 18 Variation of d_F with the Froude Number, N_{Fr}^{*}

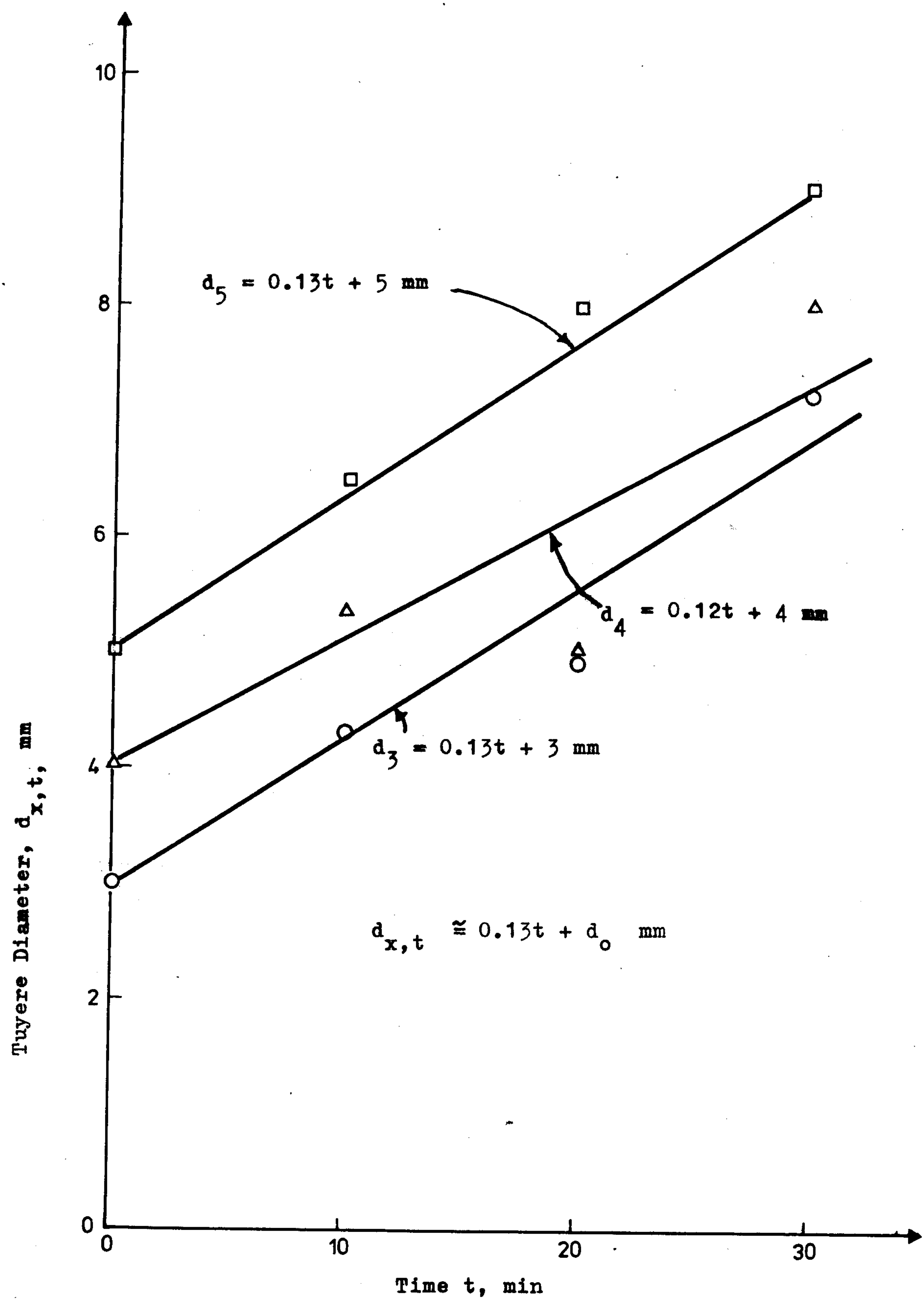

Fig. 19. Variation of orifice diameter with time at constant flow conditions i.e $N_I = 0.06$

The increase of moles of tuyere eroded as indicated by the slope of the graphs and therefore increase with N_I indicates that as the momentum force in the bubble as well as the kinetic energy increases, more erosion occurs both on the surface of tuyere and in the inner tuyere. An increase in the Injection Number at constant tuyere diameter d_σ as seen in Figure 17 means that the main parameter in the injection equation

$$N_I = \left[\frac{Q^2}{r_o^5\ g}\right]^{2/5} \quad \frac{\rho_g}{\rho_\ell}$$

enhancing the wearing mechanism is the gas flowrate Q, which also affects the gas kinetic energy. The kinetic energy varies as $KE \propto Q^2$, as such an increase in Q results in a high increase in the kinetic energy term.

If we consider that k_m, in the equation $k_\alpha = k_m A$ were a constant and dependent on the washing effect of the liquid when it fluctuates in the left to right manner on the tuyere surface, much of the overall lateral erosion will be expected to depend on the contact area of the bubble with the tuyere surface given by A which varies and is to a greater extent dependent on the gas flowrate as shown by a plot of bubble contact radius r_c, against the flowrate Q and Froude Number N_{Fr}^* where r_c increases with both parameters as shown in Figures 20 and 22.

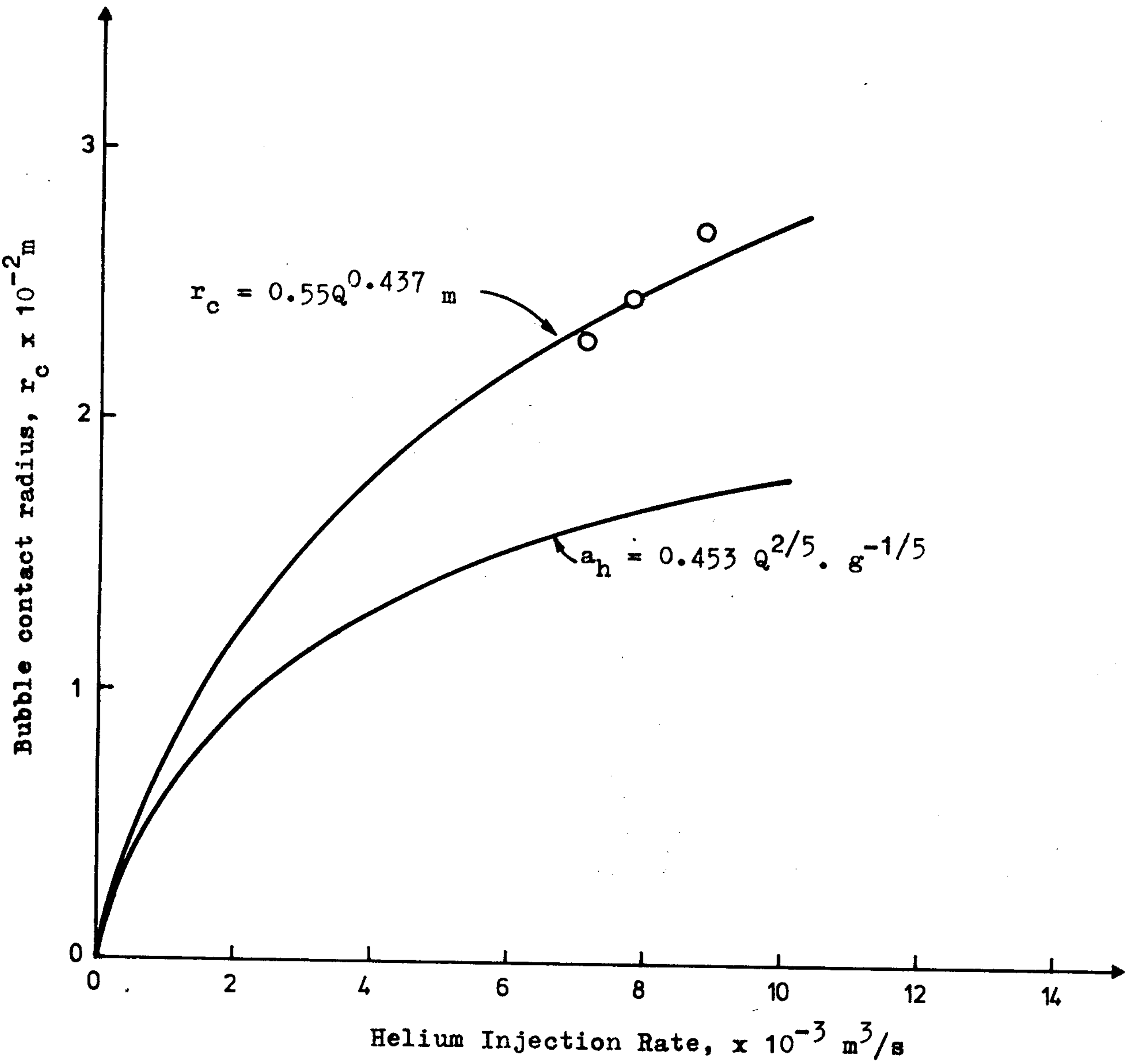

Fig. 20 Variation of bubble base contact radius, r_c with injection rate (At d_o = 4.0 mm)

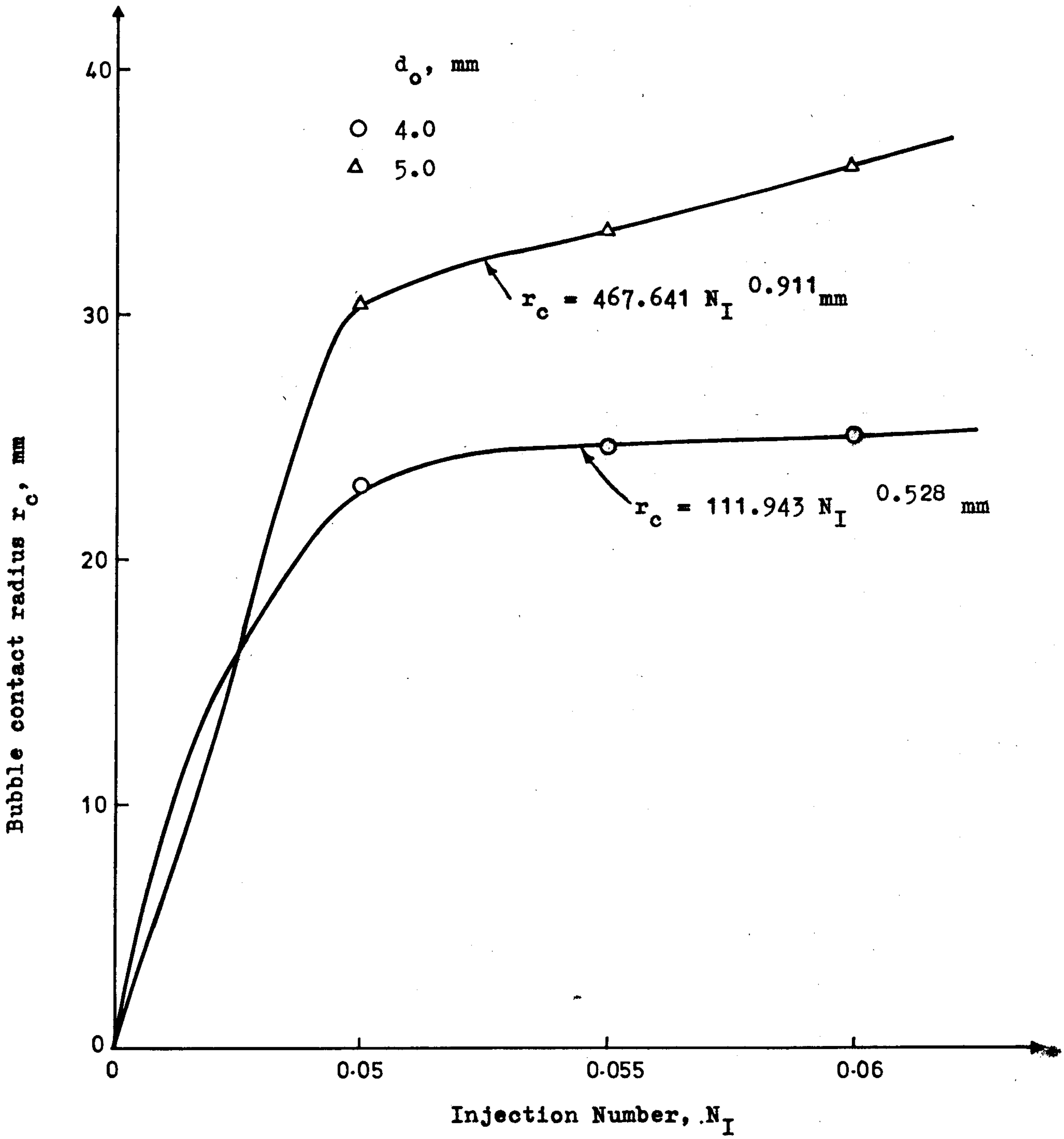

Fig. 21 Increase of bubble contact radius with Injection Number

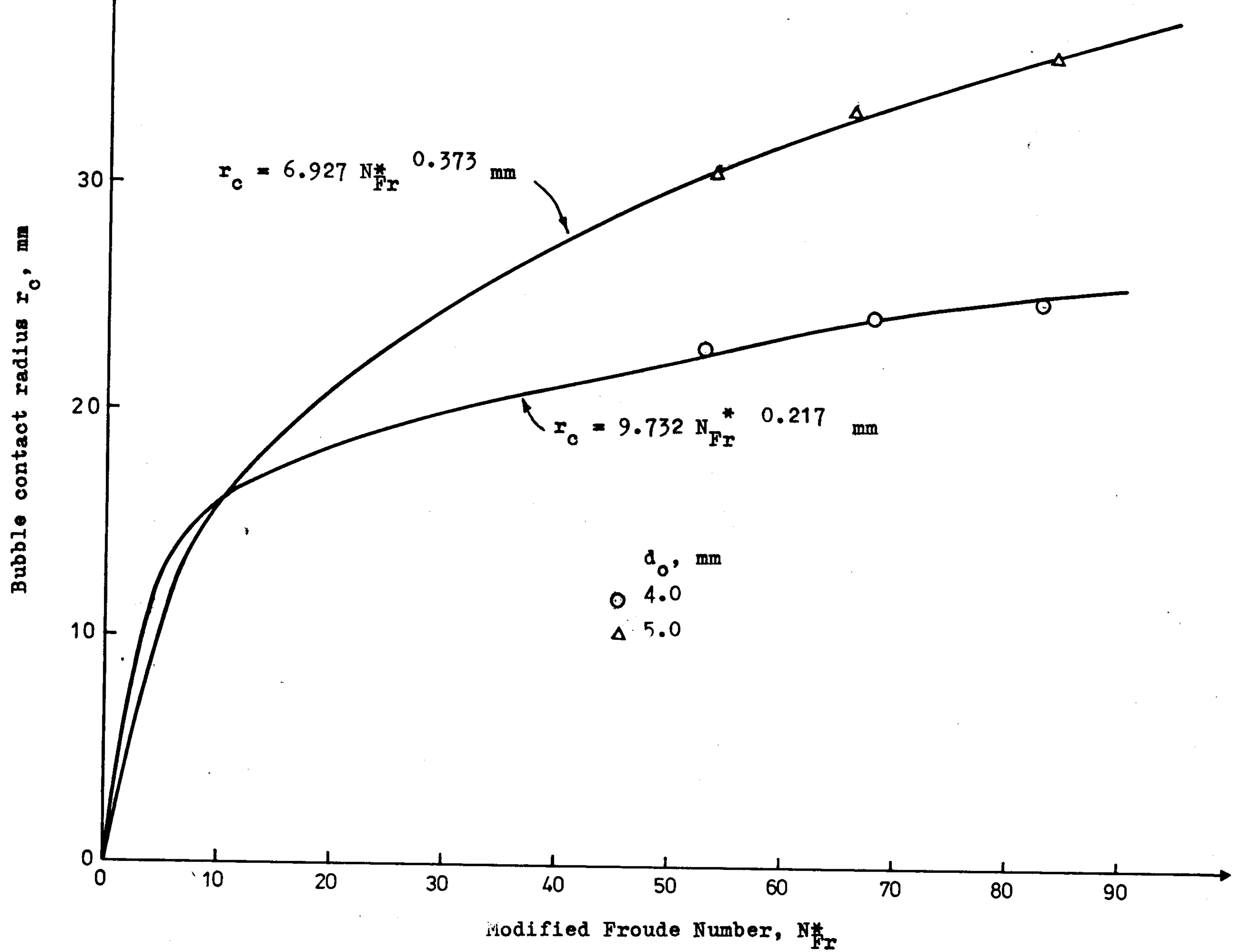

Fig. 22 Increase of bubble contact radius with the Froude Number

The effect of N^*_{Fr} as given by the plot of bubble contact radius r_c against Froude Number as seen in Fig.22 in which r_c increases with N^*_{Fr} shows that at constant tuyere diameter, erosion of the tuyere surface is also due to high inertial forces resulting from increased gas velocity at high flowrates.

The increase in bubble contact radius r_c, with the Modified Froude Number and flowrate as shown in Figures 20 to 22 which means increase in the spread or wetting on the tuyere surface which can be said to be affected by the competition of the outward surface tension forces and the inward inertial forces of the recirculating flow of the bath, shows that as the gas flow increases, promoting agitation and high convective currents, more material is eroded from the tuyere surface. The rather erratic variation and increase of r_c indicates that a stagnant layer of the fluid on the tuyere surface is almost non-existant and material will be transported into the bath mainly by eddy and turbulent diffusion.

The bubble base contact radius r_c for the Helium - Hydrochloric acid system as seen in Fig. 20 is higher than or varies from the theoretical obtained with Air-water experiments at the same flowrate because of the differences in their densities, as such, the effect of the gas momentum forces will differ and consequently affect the bubble diameter. In the present work it was found that r_c varies as

$$r_c = 0.55\ Q^{0.437} \cong 0.55Q^{2/5}$$

$$\text{i.e} \qquad r_c \underline{\propto} Q^{2/5}$$

For helium gas, the gas momentum as compared to Air is reduced and the higher inertial forces act to deform the bubble thereby increasing the bubble contact radius. Figure 23 shows that size of bubble increases with time and is affected substantially by the size of the tuyere.

Figure 18 shows that d_F increases with the Modified Froude Number N^*_{Fr}. This effect of N^*_{Fr} on the original tuyere diameter d_o shows that as the inertial forces increase, more axial erosion at the top part of the tuyere where the bubble is forming occurs because the increase in the inertial forces enhance s 'back-Attack' to occur as such it can be said that axial erosion depends to a greater extent on the high inertial forces. The dependence of the final diameter d_F on the original tuyere diameter d_o in the equation

$$d_F = 0.05N^*_{Fr} + d_o$$

Suggests an influence of the kinetic energy of the gas which is also influenced by the velocity of the gas in the tuyere.

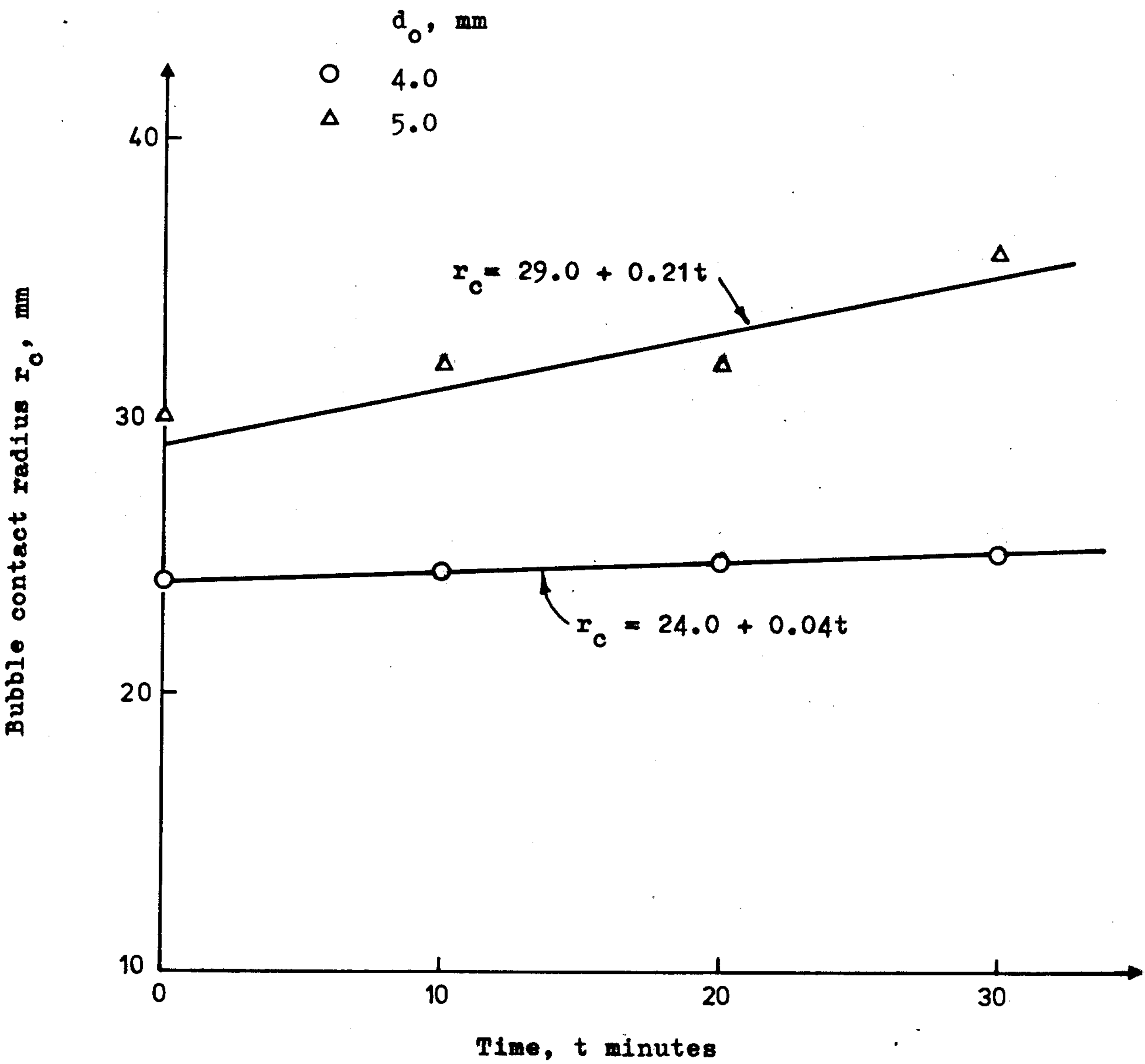

Fig. 23 Increase of bubble contact radius with time at constant Injection Number $N_I = 0.06$

2.2 Two-phase Flow Study

Two-phase flow experiments as shown in Fig. 24 to 26 show that as the injection Number increases and the flowrate increases as we go towards jetting conditions, the liquid film thickness δ_l, and percent volume of entrained liquid % V_l decreases and erosion would be expected to be minimal mostly in the inner lower part of the tuyere. In the two-phase flow experiments, the transition to a dry tuyere was observed to occur at 20% V_l. In the Injection range used in commercial practice, $N_I = 0.05$ to 0.06, we would expect to have % V_l to be in the range of 17% to 20.98%. It is interesting to note that as the diameter of the tuyere increases with time from d_o to d_F, back pressure will be expected to reduce and a reduction in erosion rate to occur, but this reduction is mostly in the bore of the tuyere and not at the top where the bubble is forming. Two-phase flow can be said to affect mainly axial erosion.

Observations from the cine films as sketched in Fig. 11, show that more liquid is plunged into the top part of the tuyere at bubble detachment. This could be due to the fact that the volumes of the bubbles and the flowrates of gas at this point are quite high as given by equation (30) enhancing what is known as 'back-attack'.

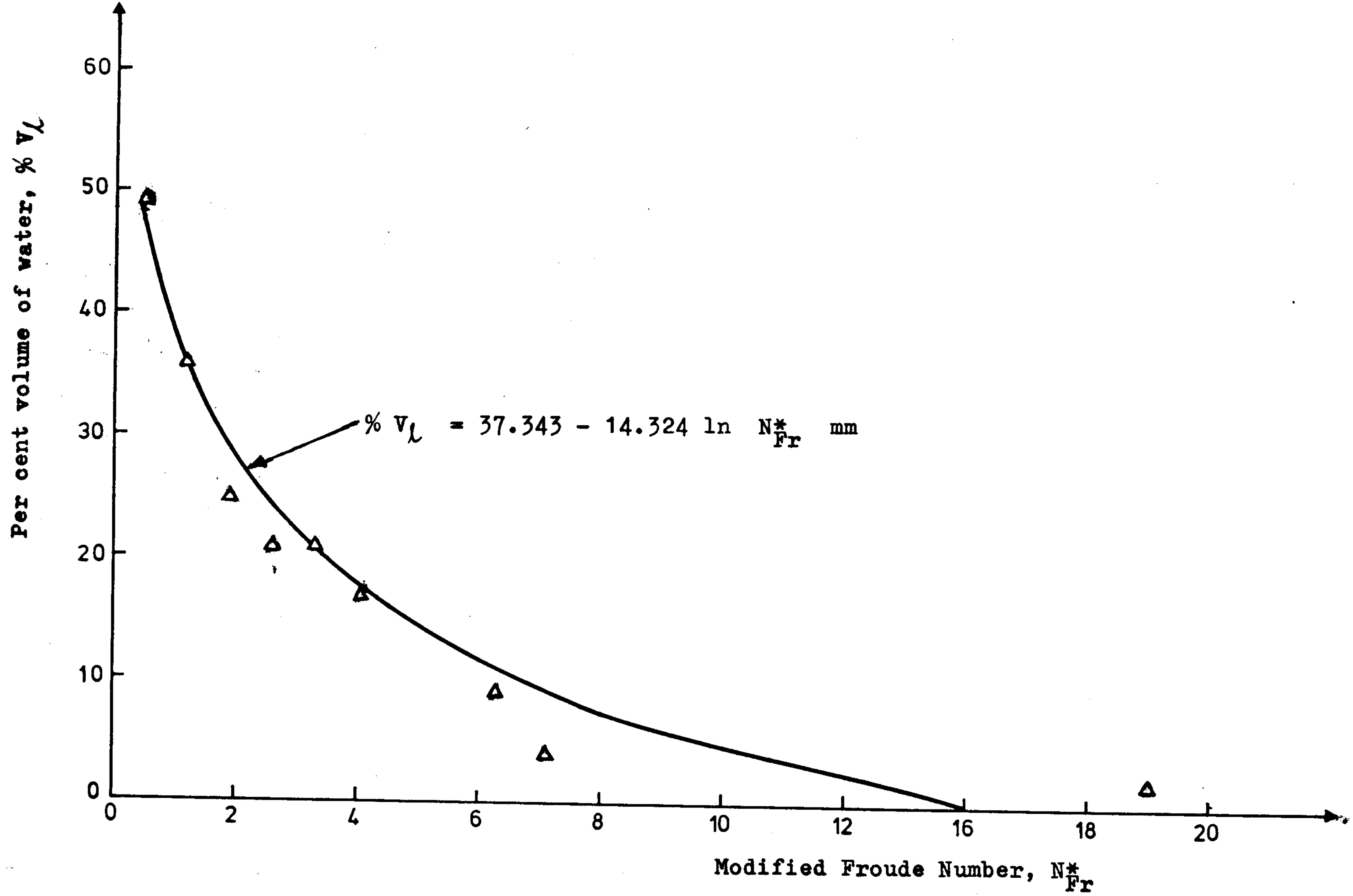

Fig. 24 Decrease of % volume of fluid with modified Froude Number at constant Tuyere diameter

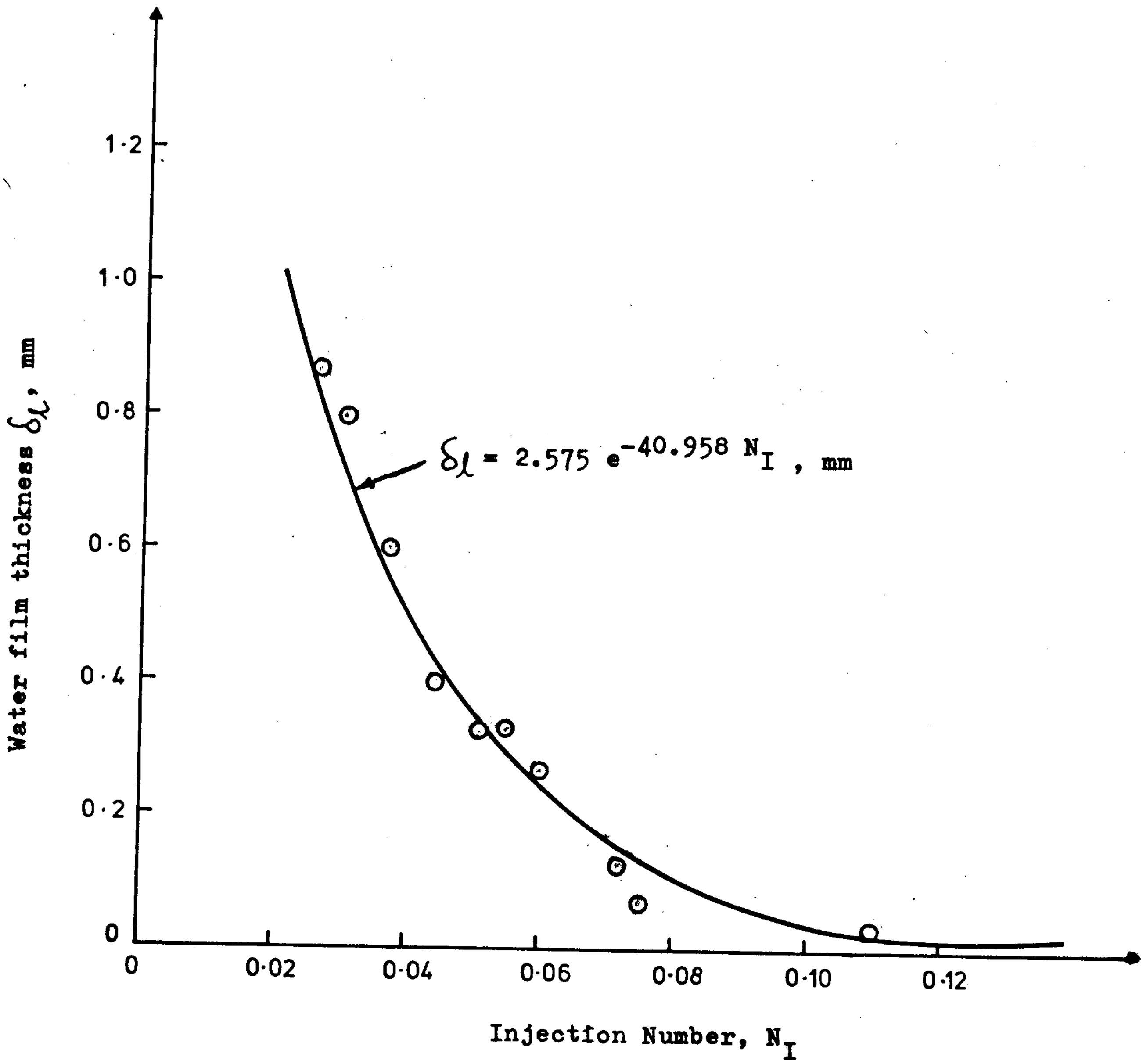

Fig. 25 **Decrease in fluid film thickness (δ_l) with increase in injection number at constant Tuyere diameter**

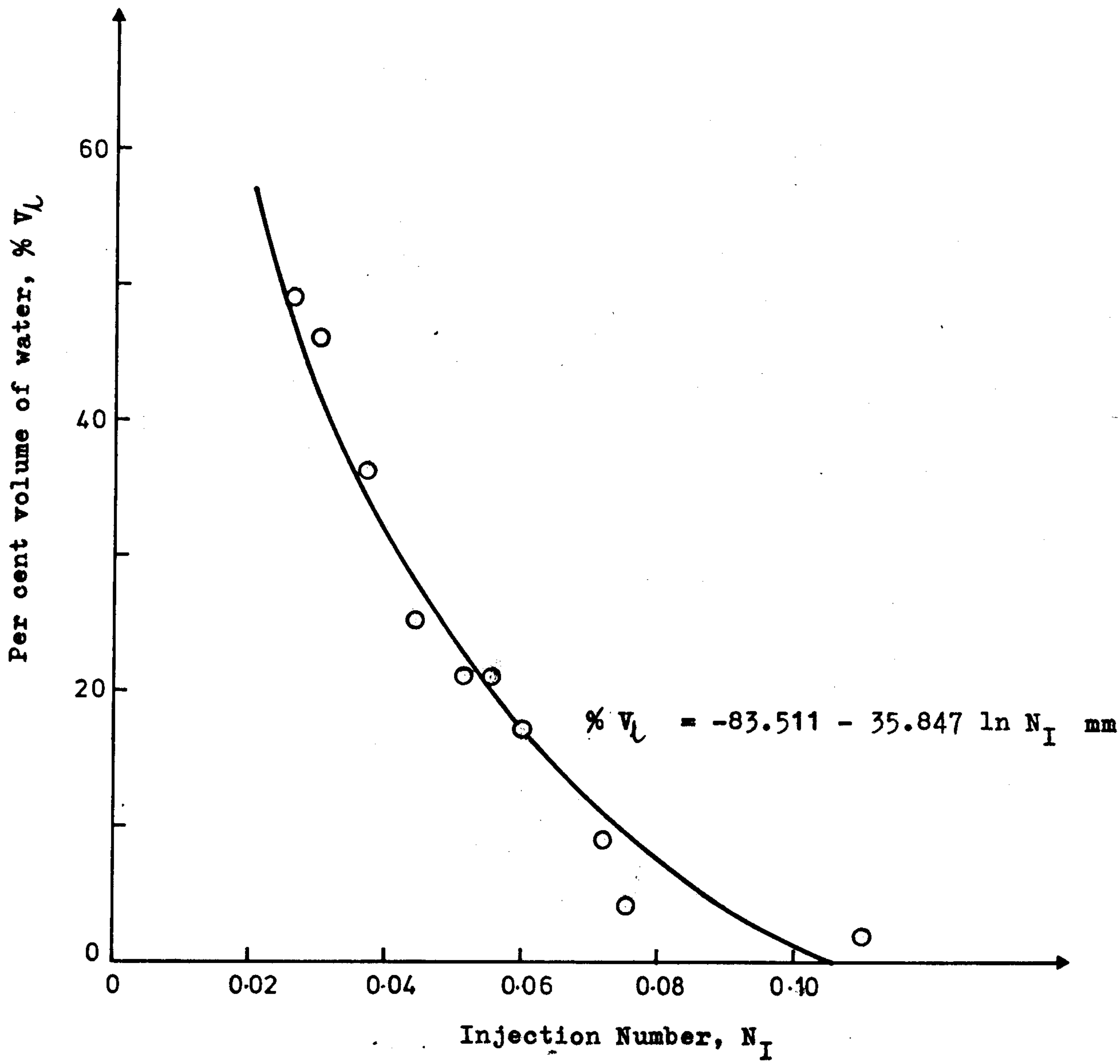

Fig. 26 Decrease in % volume of fluid with increase in injection number at constant Tuyere Diameter

2.3 A Correlation of Penetration Theory to Experimental data

If we assume that the erosion mechanism follows the Penetration theory and that the exposure time t_e which is the contact time, depends on the flowrate Q, and the Modified Froude Number N^*_{Fr},

$$t_e = fn\ (Q,\ N^*_{Fr})$$

And the bubble volume is given by eqeation (24)

$$V_B = k\ Q^{6/5}\ g^{-3/5} \cong k'\ Q^{6/5}$$

Then

$$Q \times t_e = k' \times Q^{6/5},\quad k' = k\ g^{-3/5}$$

Assuming $k = 1$

$$t_e = k' \times Q^{1/5} \cong g^{-3/5} .\ Q^{1/5}$$

According to the Penetration theory, for low concentrations of diffusing substances

$$k = 2\left(\frac{D_{AB}}{\pi t_e}\right)^{\frac{1}{2}} \qquad (56)$$

Therefore

$$k = 2\left(\frac{D_{AB}}{\pi\ k'\ Q^{1/5}}\right)^{\frac{1}{2}}$$

$$k = \frac{2\ D_{AB}^{\frac{1}{2}}}{\pi^{\frac{1}{2}}\ k'^{\frac{1}{2}}} \times \frac{1}{Q^{1/10}}$$

Let $\beta' = 2\ \dfrac{D_{AB}^{\frac{1}{2}}}{\pi^{\frac{1}{2}} .\ k'^{\frac{1}{2}}}$

Then

$$k_m = \frac{\beta'}{Q^{1/10}} \Rightarrow k_m \propto Q^{-1/10}$$

From equation (41)

$$n = -k_m A_c \Delta C t$$

$$= -k_\alpha \Delta C\ t$$

$$k_\alpha = k_m A_c$$

Where A_c = Contact area

$$= \frac{\pi}{2}\left[\left(r_c^2 - r_o^2\right) + r_o l\right]$$

Therefore

$$k_\alpha = \frac{\beta'}{Q^{1/10}} A_c$$

Considering that $r_c = 0.55 Q^{2/5}$; $r_c \propto Q^{2/5}$

$$k_\alpha = \beta' Q^{-1/10} \cdot \frac{\pi}{2}\left[(0.55)^2 Q^{4/5} - r_o^2 + r_o l\right]$$

$$k_\alpha = \frac{\pi}{2} \beta' \left[(0.55)^2 Q^{7/10} - \left(\frac{r_o^2 - r_o l}{Q^{-1/10}}\right)\right]$$

Let $C' = \frac{r_o^2 - r_o l}{Q^{-1/10}}$

$$k_\alpha = \frac{\pi}{2} \beta' (0.55)^2 Q^{7/10} - \frac{\pi \beta'}{2} C'$$

Let $\beta'' = \frac{\pi}{2} \beta' (0.55)^2$

$$C'' = \frac{\pi}{2} \beta' C'$$

Then

$$k_\alpha = \beta'' Q^{7/10} - C'',$$

which gives, for d_o = 3mm ,

$$k_\alpha = 0.0133904\ Q^{7/10} + 0.014939775\ Q^{1/10} \mathrm{cm}^3/\mathrm{sec}$$

Therefore $k_\alpha \propto Q^{7/10}$ for Penetration theory

From the obtained experimental data, the results in Fig. 27 is

$$k_\alpha \propto Q^{0.514} \quad cm^3/sec.$$

The diversion of the obtained results from the theoretical is acceptable and could be said to be due to the difference in the washing or spreading effect of the bubble which is not the case to that explained in theory. This can be said to be true because from the equation

$$k \propto D_{AB}^{n}$$

n depends on the erosion or diffusion mechanism. The equation $k_\alpha \propto Q^{0.514}$ also shows that with increased flowrate, we have an increase in the overall erosion.

The graphs in Fig. 27 show that at low flowrates, the erosion or wearing profile almost follows the penetration theory. The difference in the two curves at high flowrates could be due to a number of factors, for example; instead of one exposure cycle, we have two exposures per cycle on the tuyere surface, t_e assumed to be the exposure time is not really the exposure time for the bubble frequency. The assumption that k = 1 could differ as there is no penetration for sometime as such k could be less than one.

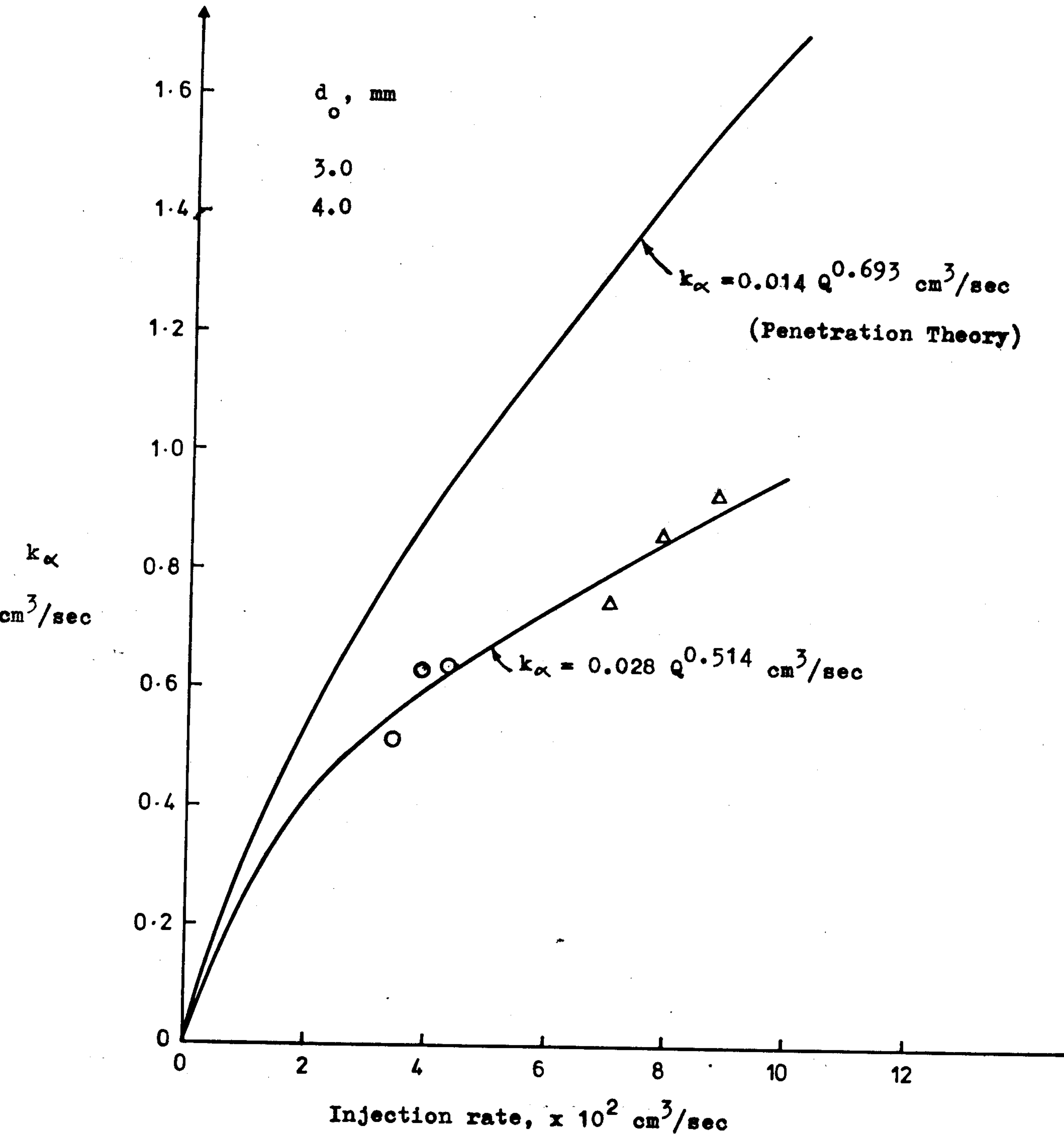

Fig. 27 Variation of k_α with flowrate

3.0 CONCLUSIONS

From the foregoing, it can be concluded that high flowrate conditions prevailing in bubbling will mostly influence lateral erosion and bulk of the erosion takes place on the tuyere surface. It can be said that high gas momentum and kinetic energy promote the overall tuyere wear as they influence the bubble contact radius r_c which varies as

$$r_c = 0.55 \quad Q^{0.437} \quad (m)$$

as well as the recirculating flow around the tuyere.

Axial erosion which is affected by high inertial forces also occurs to a great extent at detachment of the bubble. At a time when there are high inertial forces, increasing the flowrate could to some extent prevent erosion in the inner part of the tuyere as jetting conditions are approached, as the tuyere remains dry, but this would at the same time give high erosion profile at the top part of the tuyere. For a particular tuyere diameter, the final diameter will be expected to follow the equation,

$$d_F = 0.05 \, N_{Fr}{}^{*} \; + \; d_o$$

and increase at a rate given by

$$d_{x,t} = 0.1 \, t + d_o$$

The dependence of d_F on the original diameter suggests that axial erosion also depends on the tuyere dimensions and the flowrate which affect the kinetic energy of the gas.

The experimental results have also shown that the erosion mechanism to an extent follows the penetration theory.

Observing the law of similarity, the above results of the model, can be said to be representative of the actual situations occuring in commercial practice. The high viscous, tensional, momentum and inertial forces in commercial operations will promote high contact radius r_c leading to extensive lateral erosion profiles if very high modified Froude Number N_{Fr}^* values are used.

To contain the situation of high erosion profiles, it would be ideal to operate at injection numbers not much higher than N_I = 0.06 so that operations fall in the range of k_α equal to 0.65 to 0.85 cm^3/sec.

d_o (mm)	N_I	Q (ℓ/min)	INITIAL N^*_{Fr}	d_{10} (mm)	d_{20} (mm)	d_F (mm)	$d^* = \frac{d_F}{d_o}$	r_c (mm)
3.0	0.05	20.38	52.41	3.55	4.95	5.5	1.83	-
	0.055	23.11	67.4	3.88	5.0	6.75	2.25	-
	0.06	25.95	82.68	4.32	4.9	7.25	2.42	-
4.0	0.05	42.23	53.25	5.23	6.09	6.75	1.69	22.9
	0.055	47.47	67.68	5.53	6.11	7.5	1.88	24.5
	0.06	52.64	83.16	5.0	5.36	8.0	2.00	25.2
5.0	0.051	74.1	54.13	5.5	7.17	7	1.4	30.5
	0.055	81.88	66.20	6.05	7.17	8	1.6	33.5
	0.06	92.57	84.18	6.5	8.0	9	1.8	36

Notation:

d_o = Initial Tuyere diameter L

d_F = Final Tuyere diameter L

d_{10}, d_{20} = Tuyere diameter at 10 and 20 minutes L

$d^* = \frac{d_F}{d_o}$ = Dimensionless diameter ratio

N_I = Injection number

N_{Fr}^* = Modified Froude Number

Q = Gas Flowrate L^3T^{-1}

r_c = Maximum Bubble Contact radius attainable L

TABLE 2 AMOUNT ERODED WITH TIME

Time (sec)		600	1200	1800		
d_o (mm)	Q ℓ/min	Amount Eroded (Moles) x 10^{-3}			k_α cm^3/sec	Slope of straight line (moles/sec)
3.0	20.38	1.56	3.39	5.73	0.519	3.17×10^{-6}
	23.11	1.81	3.77	6.46	0.63	3.85×10^{-6}
	25.95	1.64	3.85	7.05	0.64	3.89×10^{-6}
4.0	42.23	2.36	5.57	8.03	0.745	4.55×10^{-6}
	47.47	3.69	6.52	9.57	0.86	5.25×10^{-6}
	52.64	3.37	6.57	10.125	0.93	5.68×10^{-6}
5.0	74.1	2.78	4.31	7.47	0.65	3.98963×10^{-6}
	81.88	4.01	7.03	10.08	0.96	5.84×10^{-6}
	92.57	2.8	6.86	9.85	0.91	5.57×10^{-6}

Note: Slope = $\dot{n} = k_m A_c \Delta c$ moles/sec

Let $\Delta c = 6.1 \times 10^{-6}$ moles/cm^3

$$k_\alpha = \frac{k_m A_c \Delta c}{\Delta c} \quad cm^3/sec$$

TABLE 3. TWO PHASE FLOW DATA USING WATER AND AIR

Q (ℓ/min)	N_I	N^*_{Fr}	δ mean (mm)	V_ℓ (mm^3)	% V_ℓ
4.06	0.026	0.49	0.867	167.77	49.4
4.80	0.0295	0.68	0.8	156.83	46.0
6.28	0.037	1.17	0.6	122.14	35.0
7.95	0.044	1.88	0.4	84.44	24.89
9.42	0.051	2.64	0.33	71.21	20.98
10.49	0.055	3.26	0.33	71.21	20.98
11.69	0.06	4.06	0.267	57.64	17.0
14.54	0.072	6.28	0.133	29.49	8.7
15.40	0.075	7.05	0.067	14.91	4.4
25.26	0.11	18.96	0.033	7.5	2.2

Note:-

Total volume of Tuyere = 339.29 mm^3

d_o = 6.0 mm

Length of Tuyere = 24 mm

δ mean= Mean Liquid layer thickness along inner tuyere from Tuyere wall taken at 3 points

V_ℓ = Volume of Liquid (water)

REFERENCES

1) WRAITH, A.E., "Two stage bubble growth at a submerged plate orifice". Chemical Engineering Science, 1971, Vol 26, pp 1659-1671. Pergamon Press.

2) DAVIDSON, J.F and SCHÜLLER, B.O.G. ; "Bubble formation at an orifice in a viscous liquid". Trans. Inst. Chem. Engineers Vol 38, 1960 ; pp 144

3) CHALKLEY, M.E and WRAITH, A.E: "Gas dispersion from a Tuyere in Mercury". Trans. IMM, 1978, Vol 87, C266 - 270.

4) KAKUTANI, T., and WRAITH, A.E. "Pressure beneath a growing rising bubble" Chem. Engineering Science 1974, Vol 29, pp 1 - 12.

5) KUFERBERG, A and JAMESON, G.J. "Pressure below a bubble accelerating from rest - 'Simple Theory and Applications'". Chem Eng. Science. 1967, Vol 22, pp 1053 - 1055.

6) DAVIDSON, J.F and SCHÜLLER, B.O.G. "Bubble formation at orifice in an inviscid liquid". Trans. Inst. Chem. Engineers Vol 38, 1960, pp 335 -

7) NILMANI, M and ROBERTSON, D.G.C. "Model studies of Gas Injection at high Flowrates using water and mercury". IMM Conference (1979) on "Gas injection into liquid metals". University of Newcastle-Upon-Tyne, pp B1 - 36.

8) AOKI, T, HATONO, A, MASUDA, S., and TAGA, M "Characteristics of submerged gas jets and a new type bottom blowing tuyere". IMM Conference on 'Injection Phenomena in Extraction and Refining'. University of Newcastle-Upon-Tyne, 1982, A1-36, Vol 1.

9) WRAITH.A.E, Part III 1985 lecture notes, Department of Metallurgy and Engineering Materials, University of Newcastle-Upon-Tyne.

10) BOXALL, G., SABHARWAL, A.K., ROBERTSON, T., and *HAWKINS, R.J. "Modelling and visualization of Tuyere accretion growth" - British Steel Corp - Teeside Laboratory Report.*

11) COLLINS, P. "Isothermal Model studies of the flooding characteristics of Plain and Annular Tuyeres". IMM Conference on 'Injection Phenomena in Extraction and Refining', Newcastle, 1982, D1 - 21, Vol 1.

12) CHALKLEY, M.E and WRAITH, A.E. "Gas dispersion at an Annular Tuyere", IMM Conference on 'Gas injection into liquid metals'. University of Newcastle-Upon-Tyne, 1979, D1-23.

13) WALTERS, J.K. and DAVIDSON, J.F: Journal of fluid mechanics, 1962, Vol 17, pp 321.

14) SZEKELY, J and THEMELIS, N.J. "Rate Phenomena in process metallurgy" pp 590, Wiley-Interscience, Canada 1971.

15) SZEKELY, J and THEMELIS, N.J. "Rate Phenomena in Process Metallurgy" Wiley-Interscience-London, (1971), pp 590.

16) DAVIES, J.T. "Turbulence Phenomena" Academic Press (1972) London.

17) TREYBAL, R.E. "Mass Transfer Operations" Third Edition; McGraw-Hill Book Company, (1980) USA.

18) POULSON, B. "Electrochemical measurements in flowing solutions". Paper presented at International Conference on Electrochemical Methods in Corrosion testing and Research - Manchester, January 1982.

19) GOSMAN, A.D., PUN, W.M., RUNCHAL, A.K., SPALDING, D.B., and WOLFSHTEIN, M. "Heat and Mass Transfer in Recirculating Flows" Academic Press (1969) London.

20) MARTIN, H. "Heat and Mass Transfer between Impinging Gas Jets and solid surfaces" Advances in Heat Transfer, Vol 13, Academic Press (1977) New York.

21) LIGHTFOOT, E.W., STEWART, W.E., and ANGELO, J.B., AIChE.J., 16, pp 771 (1970)

22) GOVIER, G.W. and AZIZ, K. "The flow of complex mixtures in pipes" Van-Nostrand Reinhold Company (1972) New York.

23) COULSON, J.M. and RICHARDSON, J.F. "Chemical Engineering volume one - Fluid flow, Heat Transfer and Mass Transfer". Pergamon Press (1977) Third Edition. U.K, pp 89.

24) LEIBSON, I et al "Rate of flow and mechanics of bubble formation from single submerged orifices", AIChE Jl (1956), Vol 2, pp 296 - 306.

25) HUGHES, R.R. "The formation of bubbles at simple orifices" Chemical Engineering Progress (1955), Vol. 55, pp 557 - 563.

26) ANAGBO, P.E. "Model studies of Tuyere injection for metal refining", Ph.D thesis, University of Newcastle-Upon-Tyne, (1977).

27) SZEKELY, J., and EL-KADDAH, N., SCANINJECT III Proc. Int. Conf on Injection Metallurgy, MEFOS, Lulea, Sweden (1983), Part 1, 3:1.

28) CAMPLIN, M., Final Year Project Report, Department of Metallurgy and Engineering Materials, University of Newcastle-Upon-Tyne, (1983).

A P P E N D I C E S

Plate 1(a) Lateral Spreading of Bubble at 20.38 l/min. d_o=3.0 mm

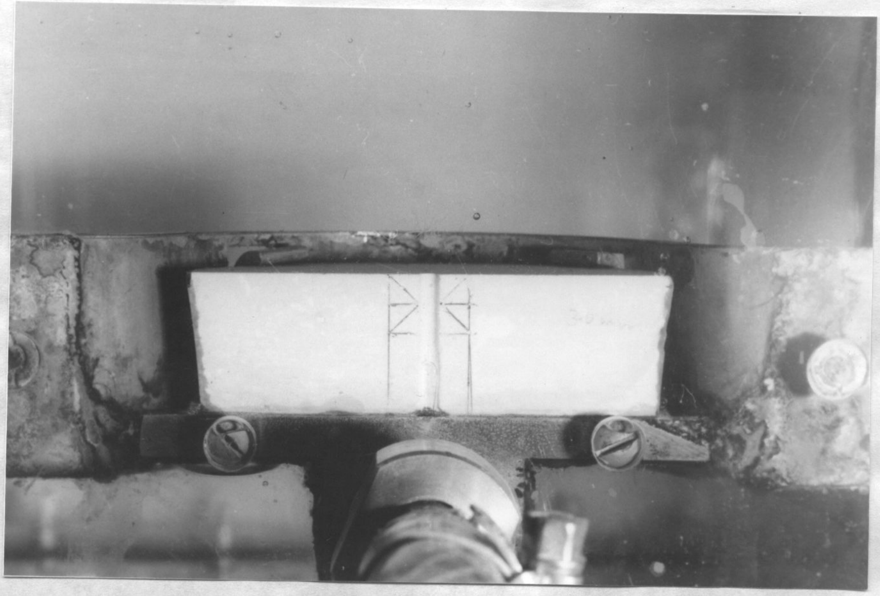

Plate 1(b) Tuyere block of d_o = 3.00 mm at start of experiment without gas injection.

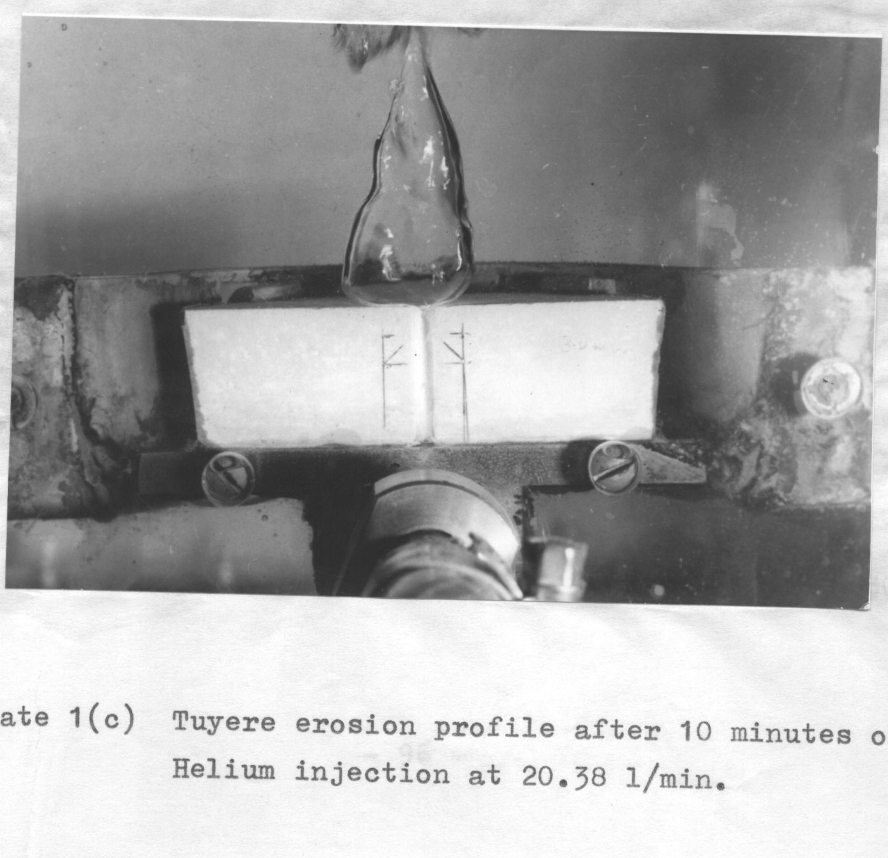

Plate 1(c) Tuyere erosion profile after 10 minutes of Helium injection at 20.38 l/min.

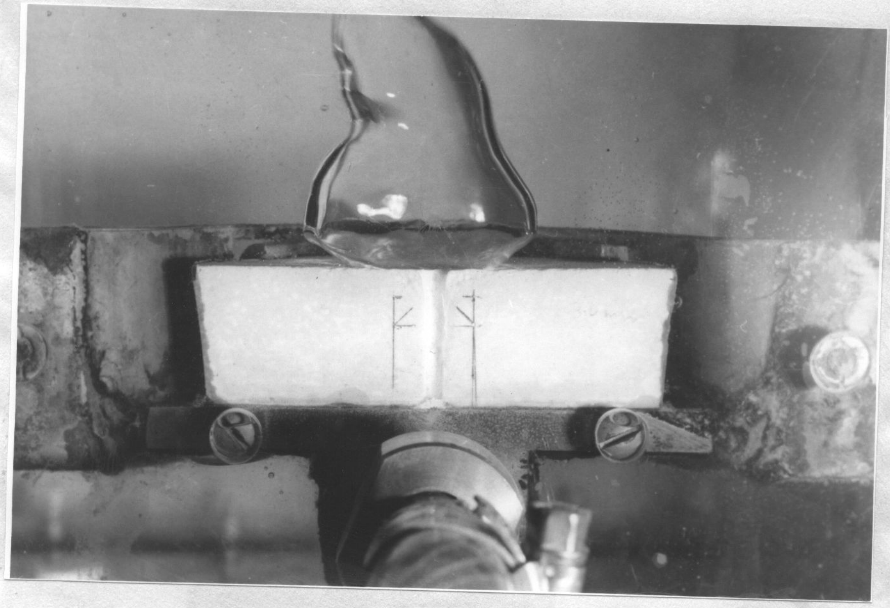

Plate 1(d) Tuyere erosion profile after 20 minutes of Helium injection at 20.38 l/min.

Plate 1(e) Tuyere erosion profile at end of experiment after 30 minutes of Helium injection at 20.30 l/min.

Plate 2(a) Bubble Coalescence Regimes

Plate 2(b) Bubble Formation sequence, variation of r_c and coalescence at Q = 20.38 l/min, d_o = 3.0 mm.